AD-A168 625 A HYDROFOIL INSTRUMENT PLATFORM FOR OBTAINING PROFILES OF OCEAN PROPERTIES(U) FLOW RESEARCH CO KENT WA D C ECHERT ET AL MAY 86 FLOW-TR-361 1/1

UNCLASSIFIED F/G 13/10 NL

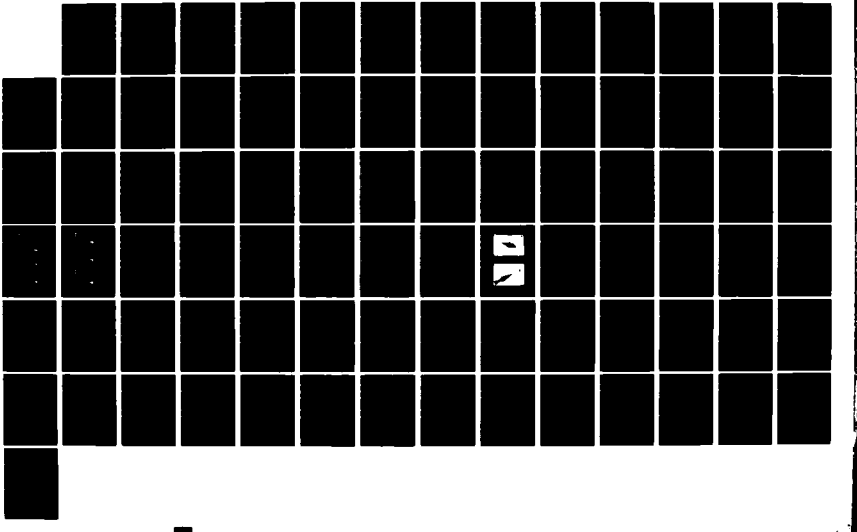

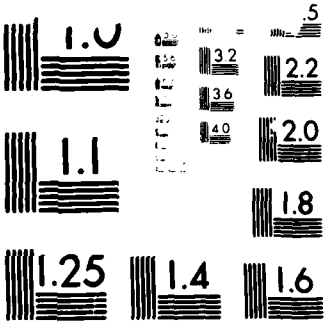
1.0
1.1
1.25
1.4
1.6
2.2
2.0
1.8

Flow Technical Report No. 361

(12)

A HYDROFOIL INSTRUMENT PLATFORM FOR OBTAINING PROFILES OF OCEAN PROPERTIES

D. C. Echert, E. W. Geller, D. J. Hanzlick, and J. H. Morison
Flow Research Company
Technology Division
21414-68th Avenue South
Kent, WA 98032

May 1986

Phase I Final Report
for Period September 1985 - February 1986
Contract No. N00014-85-C-0675

Prepared for
OFFICE OF NAVAL RESEARCH
800 North Quincy Street
Arlington, VA 22217

Unclassified
SECURITY CLASSIFICATION OF THIS PAGE

AD-A168625

REPORT DOCUMENTATION PAGE

1a. REPORT SECURITY CLASSIFICATION: Unclassified	1b. RESTRICTIVE MARKINGS
2a. SECURITY CLASSIFICATION AUTHORITY	3. DISTRIBUTION/AVAILABILITY OF REPORT
2b. DECLASSIFICATION/DOWNGRADING SCHEDULE	
4. PERFORMING ORGANIZATION REPORT NUMBER(S): Flow Technical Report No. 361	5. MONITORING ORGANIZATION REPORT NUMBER(S)
6a. NAME OF PERFORMING ORGANIZATION: Flow Research Company; 6b. OFFICE SYMBOL (If applicable)	7a. NAME OF MONITORING ORGANIZATION
6c. ADDRESS (City, State and ZIP Code): 21414 68th Avenue South, Kent, WA 98032	7b. ADDRESS (City, State and ZIP Code)
8a. NAME OF FUNDING/SPONSORING ORGANIZATION: Office of Naval Research; 8b. OFFICE SYMBOL (If applicable)	9. PROCUREMENT INSTRUMENT IDENTIFICATION NUMBER
8c. ADDRESS (City, State and ZIP Code): 800 North Quincy Street, Arlington, VA 22217	10. SOURCE OF FUNDING NOS.

PROGRAM ELEMENT NO.	PROJECT NO.	TASK NO.	WORK UNIT NO.

11. TITLE (Include Security Classification): A Hydrofoil Instrument Platform for Obtaining Profiles of Ocean Properties (U)

12. PERSONAL AUTHOR(S): D. C. Echert, E. W. Geller, D. J. Hanzlick, J. H. Morison

13a. TYPE OF REPORT	13b. TIME COVERED	14. DATE OF REPORT (Yr., Mo., Day)	15. PAGE COUNT
Final Report	FROM 9-85 TO 3-86	May 1986	75

16. SUPPLEMENTARY NOTATION

17 COSATI CODES			18. SUBJECT TERMS (Continue on reverse if necessary and identify by block number)
FIELD	GROUP	SUB GR.	hydrofoil, ocean measurement, oceanographic instrument, oceanographic sensors, profiler, Reynolds number, salinity, temperature

19. ABSTRACT (Continue on reverse if necessary and identify by block number)

This report describes the results of a study of the feasibility of a hydrofoil instrument platform to obtain profiles of ocean properties for long deployment periods. The platform employs a low-Reynolds-number, controlled, hydrodynamic lift device to "fly" the instrument package up and down the water column along a taut cable. Because the local currents will drive the platform vertically, power requirements will be low and long deployments will be possible. Also, because only a single set of sensors will be required to cover the vertical range desired, the system will be low-cost and, for most applications, expendable. Additionally, the system will provide greater vertical resolution than could be provided by a series of fixed multiple sensors. Aspects of the concept addressed by the study include platform neutral buoyancy, water density variations, minimum operating current versus platform size, direction reversal mechanisms, tethering methods, electrical power requirements, and data transmission links.

20. DISTRIBUTION/AVAILABILITY OF ABSTRACT	21. ABSTRACT SECURITY CLASSIFICATION
UNCLASSIFIED/UNLIMITED ☒ SAME AS RPT. ☐ DTIC USERS ☐	Unclassified

22a. NAME OF RESPONSIBLE INDIVIDUAL	22b. TELEPHONE NUMBER (Include Area Code)	22c. OFFICE SYMBOL
Robert F. Obrochta	(202) 696-4118	Code 425 AR

DD FORM 1473, 83 APR EDITION OF 1 JAN 73 IS OBSOLETE

Unclassified
SECURITY CLASSIFICATION OF THIS PAGE

19. ABSTRACT (Cont.)

A delta wing configuration was selected for the hydrofoil due to its high lift at low current speeds and its overall compact shape. Tow tank model tests were made to demonstrate operation at low Reynolds numbers and the operation of a passive mechanism for direction reversal. The lift characteristics of the model agreed with theory and the passive mechanism successfully changed the direction of the model at the top and bottom of the tank.

It was concluded that the concept is indeed feasible. A design for a system to be used in ice-covered Arctic seas is proposed. It would operate in currents as low as 3 cm/s and gather data over a vertical range of 300 m for periods of up to one year. Data transmission would be by the ARGOS Location and Data Collection Satellite System.

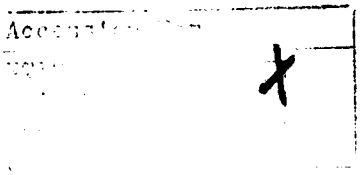

A-1

TABLE OF CONTENTS

TABLE OF CONTENTS (CONT.)

LIST OF FIGURES AND TABLES

LIST OF SYMBOLS

Symbols		Subscripts	
AR	aspect ratio	c	compensator
B	buoyancy force	core	core
b	wing span	crit	critical
C_D	drag coefficient	d	dynamic
C_{D_o}	drag coefficient at $C_L = 0$	e	elevator
C_L	lift coefficient	h	hydrofoil
D	drag	man	maneuver
d	diameter of cable	max	maximum
F	force	min	minimum
f	a fraction	o	operational condition
g	gravitational acceleration	p	payload
H	volume	s	structure, or static
L	lift	skin	skin
ℓ	length of cable segment	t	tank condition
M	resultant hydrodynamic moment	w	wing
n	load factor		
Q	current speed relative to hydrofoil		
q	dynamic pressure		
R	resultant hydrodynamic force		
S	wing area		
T	cable tension		
t	thickness of wing		
U	current speed		
V	downward speed of platform		
W	weight		
W'	weight in water		
α	angle of attack		
β	angle between platform and cable		
γ	weight density		
γ_w	weight density of seawater		
μ	coefficient of sliding friction		
ρ	mass density		
ρ_w	mass density of seawater		
θ	pitch angle		
θ_e	angle of the elevator to the platform centerline		
θ_w	angle of the wing to the horizontal		
σ	specific gravity		

SECTION 1
INTRODUCTION

The overall goal of this project, conducted by Flow Research Company (FLOW), is the development of an automatic, unattended, instrument platform capable of measuring profiles of ocean properties of interest over periods of one year. An additional objective is that the profiling platform be low-cost, thereby permitting the system to be considered expendable for most applications. The platform incorporates a hydrodynamic lifting surface that uses prevailing currents as an energy source to drive the sensor-carrying platform through the depth range of interest. This report describes Phase I of the program, which evaluated the feasibility of the hydrofoil profiler concept.

An instrument platform with both profiling capability and long endurance is important for two main reasons: (1) it will provide data on the seasonal changes in regions where, due to logistical constraints, it is impossible to attend or service the equipment, and (2) it will provide high vertical resolution unattainable with individual sensors at fixed depths. The low cost of this system relative to existing devices will permit ocean investigators to obtain higher quality data at lower cost.

This feasibility study is focused mainly, but not exclusively, on the use of the profiling system in the Arctic. This application was singled out for three reasons. The currents in the Arctic are low, if the hydrofoil platform can be made to work here it can be easily applied to other applications. Secondly, the Arctic provides severe logistical requirements on any data gathering program. The cost savings derived from the use of a hydrofoil buoy relative to alternative systems will be great. And thirdly, there is an increasing interest by both Naval and non-military researchers in obtaining Arctic oceanographic data over long periods.

For this Arctic application, the device would be suspended from a drifting ice floe. The data would be relayed by satellite from a buoy resting on the ice surface. In this way the configuration is similar to an existing buoy that the profiling buoy is intended to replace.

Morison et al. (1982) describe the development of ARGOS-based temperature-conductivity buoys, called SALARGOS buoys. The focus of their efforts has been the development of the basic technique for making unattended Arctic measurements of temperature and salinity and transmitting the data over the

ARGOS satellite system. The upper Arctic Ocean is primarily stratified by salinity because temperature fluctuations are relatively small and have little effect on density under typical Arctic conditions. Also, because salt is rejected during ice formation, buoyancy and heat flux at the surface are associated with changes in surface layer salinity rather than temperature. Thus, in order to monitor density structure, salinity must be measured. This is done by measuring both conductivity and temperature and then computing salinity. The challenge has been to obtain moored conductivity measurements uncontaminated by sensor drift due to biological fouling. The results of Morison et al. indicate this challenge can be met in the Arctic.

The SALARGOS buoy developed for these salinity and temperature measurements by Polar Research Lab (PRL) consists of an aluminum tube containing the data acquisition and transmission electronics and enough alkaline batteries to power the buoy for one year. The buoy is inserted through the ice, and sensors are suspended below the buoy on a multi-conductor Kevlar cable. In the first version of the buoy, three conductivity-temperature sensor pairs are attached to the cable at 15-m, 30-m, and 50-m depths. In a more recent version, six pairs are used.

Although the SALARGOS buoys are capable of producing useful oceanographic data, the use of fixed sensors severely limits vertical resolution and increases system cost. The objective of the proposed work is an improvement of the SALARGOS buoy by incorporating into it a continuous cycling capability. The fixed sensor string is replaced with a single sensor package that moves vertically through the water column.

The goal of the Phase I research was to find a way of achieving the automatic profiling capability for a sensor package. Possible schemes include the following: (1) a compressed-gas buoyancy float, (2) a battery-operated, counterbalanced winch, and (3) a controlled, hydrodynamic lift device. The first scheme involves inflating and deflating a bladder to raise and lower the sensors. It is similar to the technique employed in the Cyclesonde described by Van Leer (1976). This method has been shown to have endurance of at least two months. In the second scheme, a small battery-operated capstan raises and lowers the instrument package. The package is counterbalanced by a dead weight to minimize power requirements. The third scheme employs a hydrofoil to "fly" the instrument package up and down in the water column. This can be implemented with a tethered instrument (a kite configuration), as in the towed

application of Katz and Nowak (1973), or using a vertical taut cable on which the instrument rides up and down (a yo-yo configuration). For either hydrofoil deployment design, the platform uses the prevailing currents to produce hydrodynamic lift, and the only power requirement is for motion of the control surfaces. This would allow longer endurance but a less certain profiling capability due to the need for some minimum relative water velocity. Based on our review of these techniques, we have selected the hydrofoil using the taut cable as being the most feasible.

This report summarizes the Phase I effort. Section 2 presents the basic technical requirements and model assumptions for a hydrofoil profiling platform. Results of our theoretical analysis and design development of the profiler are given in Section 3, and results of tow tank experiments using models based on the theoretical findings are given in Section 4. Details of the proposed prototype system are given in Section 5. Conclusions of this study are given in Section 6.

SECTION 2

CONCEPTS AND TECHNICAL CONSIDERATIONS

In this section, the specific technical requirements and assumptions made to determine the feasibility of developing a practical hydrofoil profiling device are discussed. This device would provide a low-cost means of obtaining hydrographic data for extended periods of time. In this application, regularity of sampling and high data rates may be sacrificed for endurance and reliability.

In the following, sampling requirements are discussed, assumptions for a model design are made with respect to instrumentation and oceanic conditions, and the two configurations considered for the profiling instrument are described. The information presented in this section describes the hydrofoil profiler design philosophy used for the Phase I theoretical and experimental feasibility study.

2.1 Sampling Requirements

The measurement objective for the design of the hydrofoil profiler is to provide an average of at least one good daily profile of temperature, salinity, and pressure over a period of one year. The vertical resolution should be as fine as 2 to 5 m, and the depth range should be up to 300 m. Temperature, conductivity, and pressure should be recorded to 16-bit accuracy. This has proven to be an adequate requirement in previous SALARGOS buoys. For each sample requiring temperature, conductivity, pressure and perhaps time at 8-bit accuracy, the minimum data rate, n_{min}, is

$$n_{min} = (150 \text{ samples/cast})\ (56 \text{ bits/sample}) = 8400 \text{ bits/cast}.$$

This is also the minimum number of samples per day.

It is assumed that the data will be telemetered from the buoy using the ARGOS system. The system is arranged such that a buoy transmits an identification code and data at intervals of about one minute. These transmissions may be received by one of two or three satellites that may be passing over the site. The data are stored and the Doppler shift of the transmitted signal is measured by the satellite. This information is subsequently relayed to a ground station, and the Doppler shift data are processed to determine the buoy's position. The position and data are then disseminated to the system

user. This system has already found widespread use in the Arctic for determining ice drift, meteorological conditions and oceanographic conditions.

As a rule of thumb for the Arctic, a single ARGOS satellite makes one pass every 101 minutes or 14.25 passes/day, and during each pass a buoy can make 10 good transmissions of 256 bits at one-minute intervals. This results in a maximum ARGOS data rate of 36,480 bits per day. Thus the number of bits, n_{min}, required per cast (or per day) can be transmitted through ARGOS 4.3 times per day. In fact, there are usually two satellites operating so that if the equivalent of 4 casts per day were transmitted, they would usually all be received twice. The design scheme should thus call for sampling 4 casts per day. Under optimum conditions, an average time resolution of 6 hours would then be obtained with a safety factor of 2. In the worst case, one profile each day would get through ARGOS with a safety factor of 4.

2.2 Instrumentation Requirements

For this study, we have focused on a simple instrument package that includes only conductivity, temperature, and pressure sensors. The profiling platform could be fitted with numerous other types of oceanographic sensors depending on the mission of the platform. Even with this limited suite of sensors, the profiler will be able to measure current speed profiles. Current speed will be indicated by the vertical velocity of the platform, as measured by the change in pressure with time. Therefore, the platform would serve as a low-cost current profiling instrument. Current direction could be sensed with an on-board compass.

On-board electronics must include a microprocessor controller for directing both the operation of the sensors and the transmission of data from the profiler. The design must include provisions for data transmission hardware if the interface between the profiler and the surface is nonhardwired. A microcomputer and servo must also control the ascent/descent function of the hydrofoil if an active control system is used. Finally, the design must accommodate any battery packages necessary for power.

The sensors chosen were the Sea-Bird Electronics Model SBE-4 conductivity meter, the Model SBE-3 oceanographic thermometer, and the Paroscientific Model 8600 digiquartz depth sensor for a representative sensor package. All have been used extensively in previous oceanographic work and have acceptable performance specifications. These three sensors have a combined weight in air

of 31.76 N and a total volume of 1416 cm^3. Sea-Bird is currently developing a combined sensor package with internal recording capabilities that would be appreciably smaller than the total of the individual sensors. The microcomputer will be solid-state and therefore very compact.

The microcomputer and all sensors can operate at 12 VDC. The pressure sensor draws about 1 mA, while the other sensors draw about 10 mA. The microcomputer and servo are expected to draw 10 mA when active, but only about 1 mA when quiescent. It is estimated that any data transmission hardware on board the profiler would require 10 to 30 mA at most when active.

Sampling considerations and power budget for a prototype profiling platform are covered in detail in Section 5. In brief, the total power requirement for the controller and sensors is about 30 A-hr per year. Three packs of four lithium cells each, comprising a total volume of about 850 cm^3, can meet this requirement. Even doubling this estimate to include data transmission hardware yields a requirement that can quite reasonably be met, even in the case that all power for the profiler-borne equipment must be carried on board.

The total payload consisting of sensors, electronics, and batteries will have an estimated volume and weight of 2560 cm^3 and 55 N, respectively. Volume and weight are not such severe constraints for the surface buoy (mounted on the ice in Arctic applications) that receives data from the profiler and transmits the data to passing satellites. Again, deferring to the more detailed discussion in Section 5, the estimated power requirements for the surface buoy are about 100 A-hr per year at 12 V minimum. These requirements can be met by seven standard Polar Research Labs alkaline battery packs, which would total about 14,000 cm^3 or roughly 0.5 ft^3.

2.3 Oceanic Conditions

Obviously, the world's oceans exhibit a wide variety of regimes. Primarily Arctic applications are addressed in this study, although the profiler could easily be used elsewhere with minor, if any, modifications. Because of the low current velocities in the Arctic, it is the most severe test of the feasibility of a hydrofoil profiling system. Perhaps the most likely changes for use outside the Arctic would be in the mooring configuration rather than in the instrument itself.

For Arctic applications, the following set of environmental and performance parameters apply:

(1) The profiler should be able to sample the upper 300 m of the water column.

(2) The profiler should be able to operate over a current speed range of 0.03 to 0.60 m/s.

(3) The profiler must be able to generate enough lift to overcome changes of its weight in water due to temporal or spatial changes of 0.4% in the water density.

(4) The system must operate at low temperatures corresponding to the freezing point of seawater, about -2°C.

(5) The system must be able to withstand air temperatures of -40°C during deployment.

The 300-m depth range extends through the surface mixed layer and down to the Atlantic layer in the Arctic Ocean. The speed range is typical of ice velocities (and thus relative water velocities) that might be expected in the Arctic. The estimate of a maximum seawater density change of 0.4% due to temporal and spatial variations is based on previous oceanographic observations in the Arctic (e.g., Coachman and Aagaard, 1974). The minimum temperature constraint is obvious. Fig. 1 shows an average Arctic density profile for an expected annual deviation.

Applications in other oceanographic regimes may necessitate modifying the profiler to accommodate other environmental and performance parameters. For instance, in a shallow water environment such as over the continental shelf, the depth range would be less, currents might be greater, and the density variation might be larger than 0.4%. The profiling system described in this study is easily adaptable to the wide range of conditions that might be encountered outside the Arctic. Non-Arctic applications are discussed in Section 5.7.

2.4 Profiler Configuration

Two different tether/profiler configurations were considered for achieving the stated sampling goals. For both cases the platform becomes an underwater lifting surface (i.e., a hydrofoil) to produce vertical motion. One of the concepts was that of a hydrofoil tethered like a kite by a conducting cable. Fig. 2 shows a sketch of the configuration. The cable would extend downward

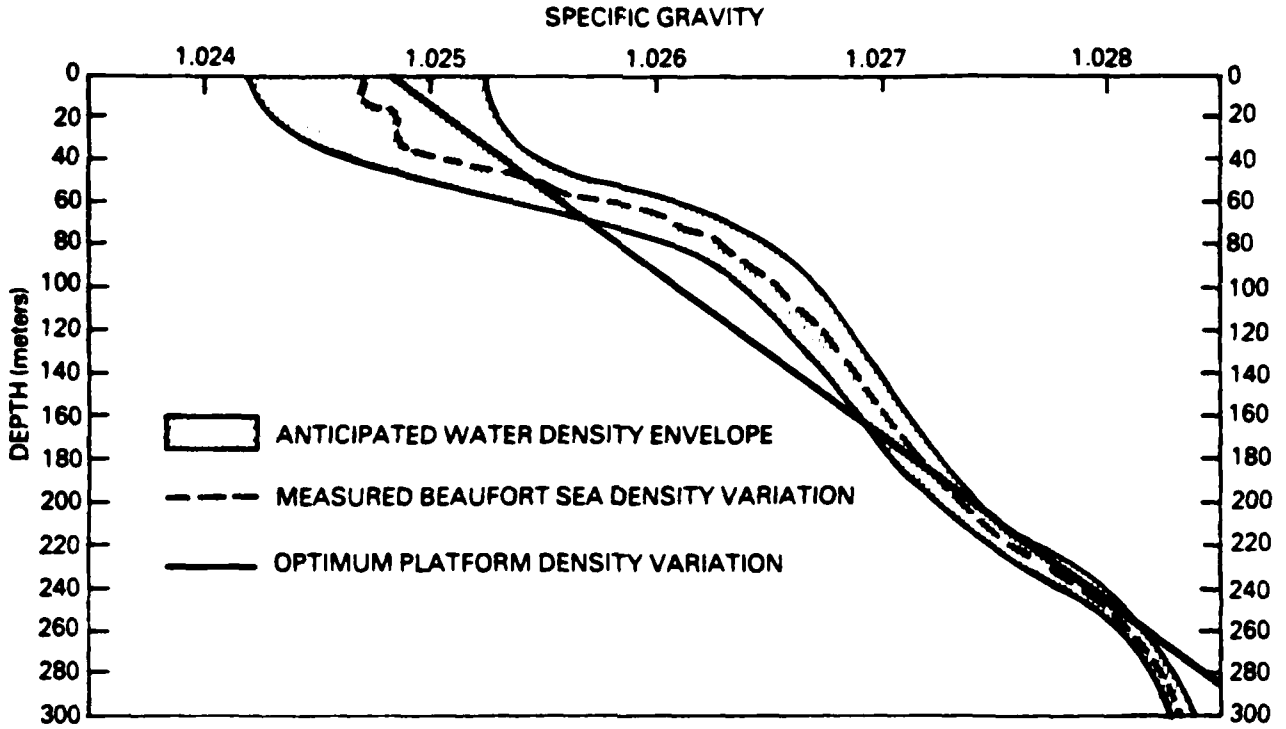

Figure 1. Water Density Envelope

11000-69

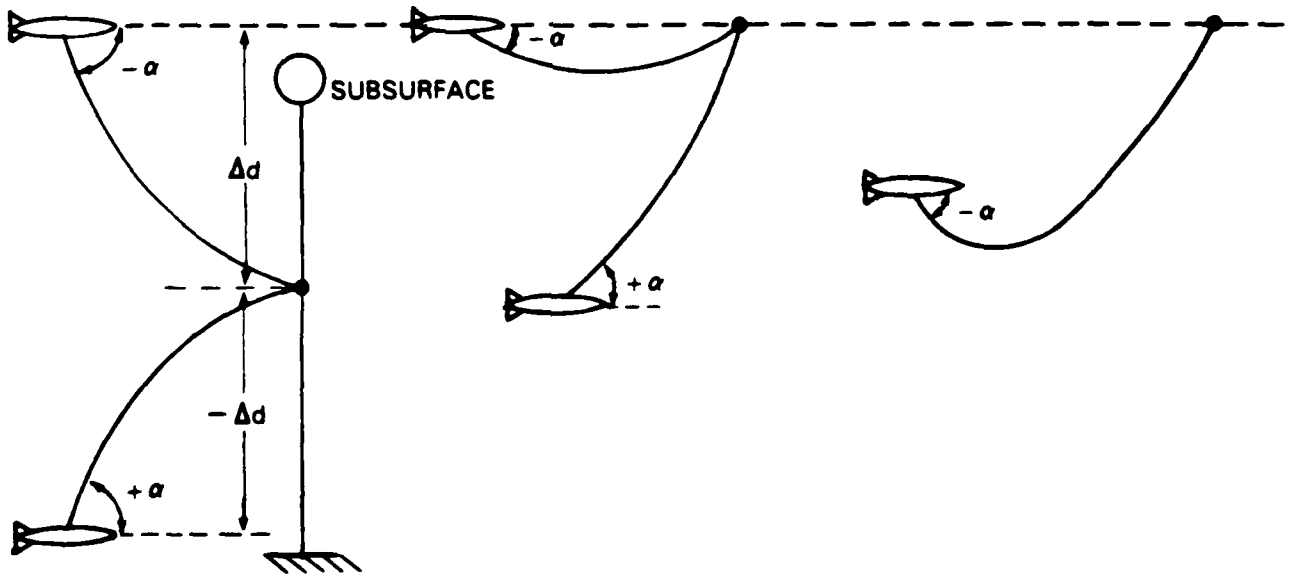

(a) Mid-depth tether

(b) Top tether (positive and negative excursions)

(c) Top tether (case where system cannot achieve shallow depth objective)

11000-65

Figure 2. Possible Kite Configurations — Distances above tether point are positive; distances below are negative. Positive and negative angles are as indicated.

from a top tether on an ice floe in the Arctic, and the profiling platform would ascend and descend in the water column by changing its angle of attack. Changing the angle of attack would be accomplished by actively moving a control surface on the profiler. Depth information from the pressure sensor would be used to determine when to actuate the controls to reverse the vertical direction of the profiler's motion. The device could be tethered either to the bottom or at mid-depth on a fixed-point taut-wire mooring or, in the Arctic example, from an ice floe. Hardwire connection to the surface through the tether cable would greatly simplify delivering power to the sensors and controls and sending data from the sensors to the surface. For brevity in subsequent discussions, this tether cable/instrument platform combination will be referred to as the "kite".

The other concept that was considered is a profiler that travels vertically up and down a taut wire either suspended from the top or moored to the bottom. This configuration will be referred to as the "yo-yo" in subsequent discussions. For Arctic applications, the device would be suspended from an ice floe, relying upon ice movement to provide the relative currents necessary for the profiling hydrofoil to generate lift. For open-ocean applications, a drogue could provide the necessary relative currents. As in the kite configuration, the direction of vertical motion of the yo-yo profiler would be determined by the angle of attack of the hydrofoil, and this would be controlled by an elevator (i.e., a pitch control surface). With the yo-yo configuration (see Fig. 3), control could be either active (similar to the kite) or passive. A passive system would incorporate a bumper in the shape of a ring attached to the cable at the top and bottom limits of the sampling depth range. Traveling vertically, the platform would encounter the bumper and, through proper coupling, the momentum of the platform would be used to alter mechanically the setting of the elevator and reverse the direction of travel. This passive method has been demonstrated successfully in tow tank tests, which will be discussed in Section 4. The yo-yo configuration would require acoustic transmission through the water or inductive transmission along the vertical guide wire in order to transmit data to the surface. There would be a need for on-board power for the electronics.

Both the kite and yo-yo configurations were evaluated to determine their feasibility as workable approaches to addressing the design and performance

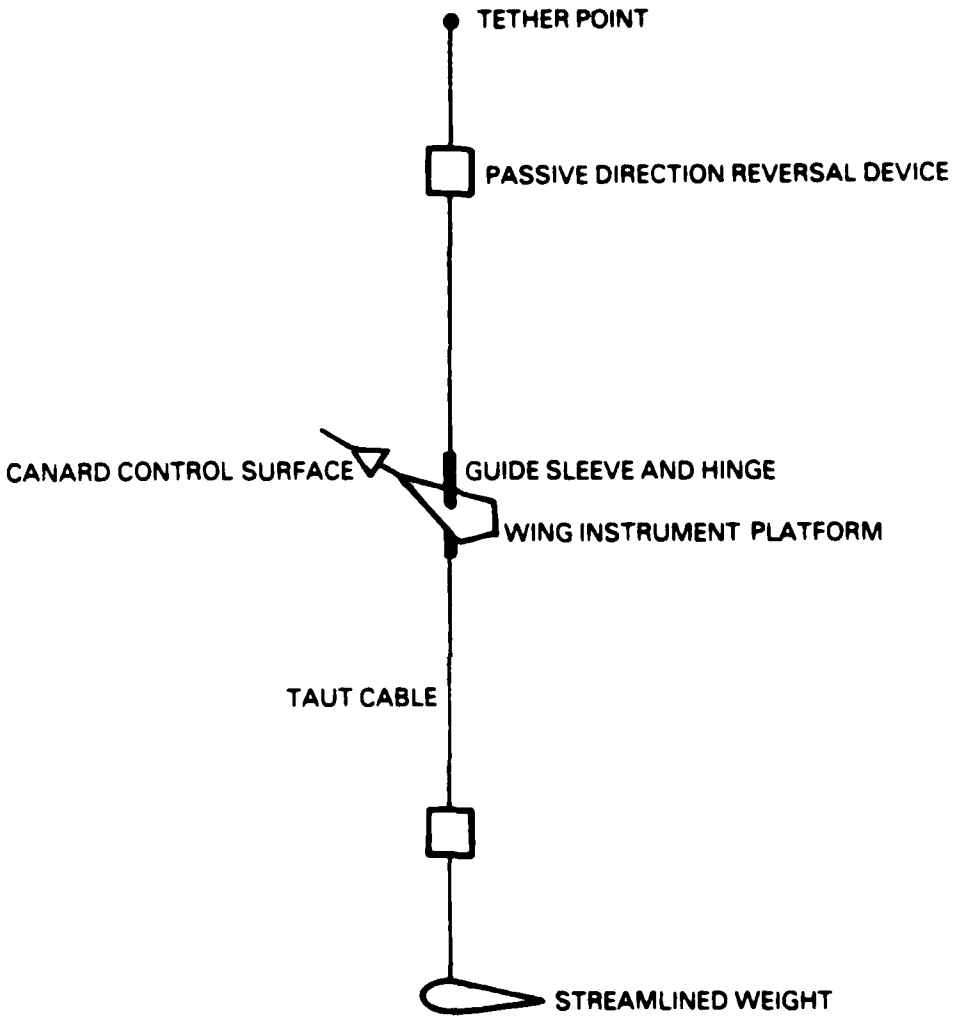

Figure 3. Yo-Yo Configuration

goals for a passive (or nearly so), inexpensive, and reliable oceanographic vertical profiling platform. These evaluations and results are described in subsequent sections of this report. In brief, it has been concluded, based upon extensive investigation including computer analysis, that the kite design constitutes a workable concept for a vertical profiler, but that it also has several limitations. The kite design may be better suited to shallow, higher current applications using a mid-depth tether rather than to lower current speed, top or bottom tether applications. In contrast, the yo-yo configuration shows considerable promise for the intended applications and could easily be extended for use in other applications.

In view of the results of the evaluation of possible profiler configurations, the Phase I effort focused on determining the feasibility and performance characteristics of a hydrofoil profiling device in the yo-yo configuration. The development and design considerations for such a profiler are discussed in detail in Section 3. The discussion includes a theoretical analysis of the performance of the yo-yo profiler. The analysis and modeling effort conducted to evaluate the kite configuration is documented in Appendix A.

SECTION 3

DEVELOPMENT AND DESIGN OF A HYDROFOIL PROFILING PLATFORM IN THE YO-YO CONFIGURATION

3.1 Design Specifications and Desirable Features

This design study for the hydrofoil profiling platform used the following specifications:

- The platform must be able to traverse the cable for current speeds as low as 3 cm/s within the ocean density envelope specified in Fig. 1.
- The payload (instruments, controller, and batteries) weight and volume are 55 N and 2560 cm^3, respectively.
- The platform must be strong enough to withstand maneuver loads at current speeds up to 60 cm/s.

The design was driven by these desirable features:

- Small size.
- Simple, inexpensive construction.

3.2 Delta Wing Configuration

A delta wing was chosen for the lifting shape of the hydrofoil because of the following advantages not inherent in a conventional wing shape:

(1) It exhibits no degradation in the maximum lift coefficient at very low Reynolds numbers.

(2) It is effective at very low aspect ratios.

(3) The airfoil shape is not important--a flat plate will do.

These three features result from the fact that a highly swept delta wing at very high angles of attack relies on vortex lift, an entirely different lift mechanism than that for a conventional wing. Vortex lift is created by large-scale vortices above the wing that reduce the pressure (see Fig. 4). These vortices are generated by separation along a highly swept wing leading edge. A sharp leading edge is not detrimental and, in fact, promotes separation at the leading edge. The airfoil shape is nearly irrelevant at high angles of attack, the only requirement being that the leading edge be sufficiently sharp to fix separation there. A flat-plate airfoil is quite satisfactory. Since the entire vortex lift phenomenon is driven by separation at the leading edge,

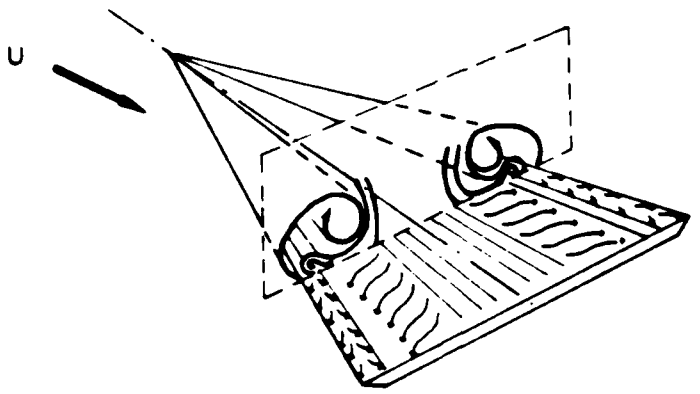

Figure 4. The Vortex Flow that Produces Lift on a Delta Wing

and since this occurrence does not depend upon the Reynolds number if the leading edge is sharp, the lift for high angles of attack of a highly swept delta wing does not drop off at the very low Reynolds numbers associated with operation of the profiling platform.

The preceding features of the delta wing translate into several advantages. The ability to use a flat-plate airfoil leads to a simple, inexpensive wing construction. The wing size required for operation in very low currents is smaller than for a traditional wing, for which Reynolds number effects reduce maximum lift. And, finally, the lower aspect ratio would translate into less wing span for the required wing area. Thus a smaller hole is needed for deployment of the profiler through an ice cover.

3.3 Lifting Requirements and Impact on the Design and Sizing

Since it is not possible to maintain neutral buoyancy over the entire operating cycle for the platform, it is necessary to generate lift to enable vertical traversing. Although the deviation from neutral buoyancy can be made very small, the lifting capability is the main design problem since the currents available to generate lift are extremely small. Of course, a wing can always be made large enough to generate a specified lift in a specified current speed. The main goal for the hydrofoil design is to minimize the wing size. Careful attention to characteristics that impact this sizing will provide significant reduction in size. Integration of the instrument packaging, the hydrodynamic design and the structural design are important. The end result is a platform that is carefully "tuned" in buoyancy to its environment.

If the platform is neutrally buoyant, then it can generate sufficient lift to traverse no matter how small it is and how low the current. However, neutral buoyancy is not possible at all times because of spatial and temporal variations in water density and changes in platform density from water absorption during long-term deployment. We explain in the following how the maximum deviation from neutral buoyancy during the annual operating cycle dictates the size of the hydrofoil, and we discuss features or characteristics of the platform that can be used to minimize its size. First, however, we discuss the spatial and temporal water density variation for the platform operating environment and the variation of the platform density that occurs with the use of buoyancy compensation.

3.3.1 The Variation in Water Density and Platform Density

The density of the Arctic Ocean varies with depth and with time over an annual operating cycle for the platform. The envelope of this variation is illustrated in Fig. 1 (from Morison and Smith, 1981). Near the surface, the density gradient is large as is the temporal excursion. It is in this mixing and melt region that water conditions vary the most.

The density of the platform is constant unless a buoyancy compensator is used. With proper choice of compensator size and compressibility, the volume of the platform and hence its density can be set at any values at the top and bottom of the excursion. A desirable variation is illustrated in Fig. 5. The objective is to minimize the maximum difference between platform density and water density.

3.3.2 Lifting Performance and the Sizing Equation

The size of the hydrofoil is dictated by the requirement of a minimum current speed for profiler operation. In that regard, the worst condition occurs at maximum deviation of water density from platform density. At maximum deviation, the weight in water is maximized (in magnitude) as is the lift required for operation. The latter is given at the critical condition by

$$L = C_{L_{max}} \frac{1}{2} \frac{\gamma_w}{g} U_{min}^2 S \quad . \tag{1}$$

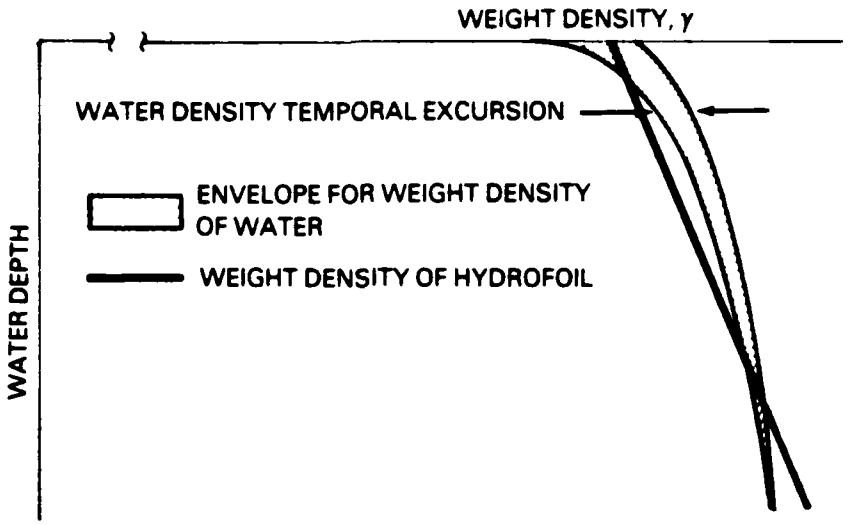

11000-67

Figure 5. Density Variation for the Water and the Platform

For a traverse to occur,

$$L = |W'| \pm \mu D \tag{2}$$

where the weight in water, W', is

$$W' = W - B = (\gamma_h - \gamma_w)H \quad , \tag{3}$$

and μ is a coefficient relating sliding friction to the drag D. If we neglect the last term in Equation (2), an approximation for the size of the hydrofoil is obtained:

$$S = \frac{2g}{C_{L_{max}} U^2_{min} \gamma_w} \cdot \left(\gamma_h - \gamma_w\right)_{max} H$$

$$\simeq \frac{2g}{C_{L_{max}} U^2_{min}} \frac{\left(\gamma_h - \gamma_w\right)_{max}}{\bar{\gamma}_w} \bar{H} \quad . \tag{4}$$

The approximate relation in Equation (4) results from the following approximations:

$$\gamma_w \simeq \bar{\gamma}_w$$
$$H \simeq \bar{H} \qquad (5)$$

where the overscore ($\bar{}$) symbolizes the mean value of the variable. These approximations are very accurate since water density and platform volume vary only a fraction of a percent from the mean. The platform volume in fact is nearly fixed unless buoyancy compensation is used.

The impact of Equation (4) on the sizing and design of the hydrofoil is shown in Sections 3.4 and 3.5. According to Equation (4), to minimize S, we need to minimize the maximum difference between the water and platform densities and to minimize the platform volume. After considering the case where no buoyancy compensation is used, we will discuss the additional size reduction that may be possible with its use.

3.4 Design Without Buoyancy Compensation

With no buoyancy compensation the platform volume does not change with depth, so

$$H = \text{constant} = \bar{H}$$
$$\gamma_h = \text{constant}$$

and Fig. 5 specializes to Fig. 6.

In the following it is convenient to divide the platform into two parts: the payload, which is fixed in size and weight, and the structure, which is the remainder and is to be sized by the design procedure. The subscripts p and s are used respectively for the payload and the structure. Also, for these approximate preliminary design calculations, it is appropriate to assume that the structure consists only of the wing. The weight and buoyancy of the boom, canard, and fin are neglected. Thus, an example regarding terminology is that W_s is the weight of the structure or approximately the weight of the wing.

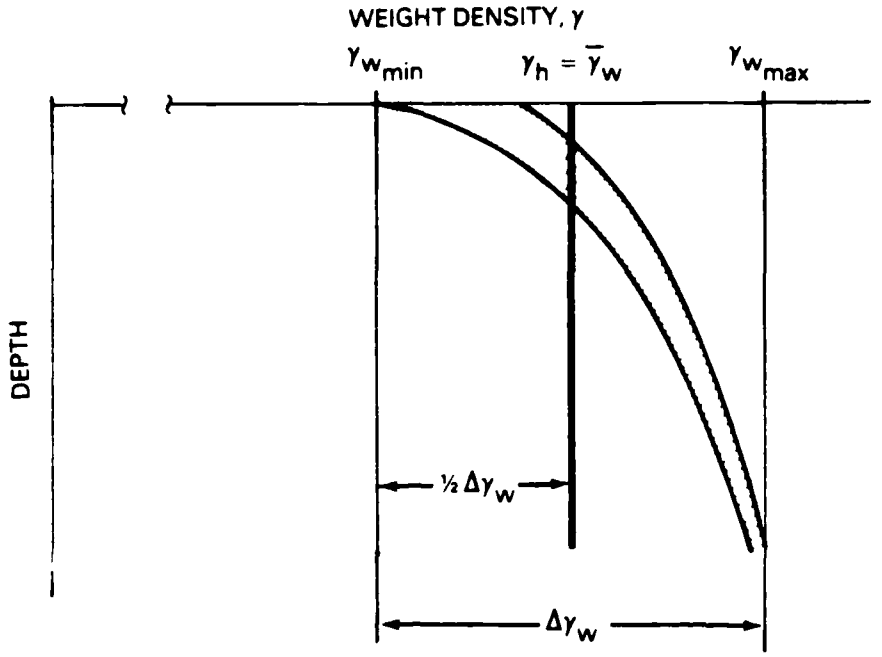

11000-66

Figure 6. Choice of Platform Density for the Case Without Buoyancy Compensation

3.4.1 Sizing and Buoyancy Equations for Optimum Platform Density

To minimize the excursion of γ_w away from γ_h, the platform is designed such that

$$\gamma_h = \bar{\gamma}_w = \frac{1}{2}\left(\gamma_{w_{max}} + \gamma_{w_{min}}\right), \tag{6}$$

so that for Equation (4) we can use

$$\left(\gamma_h - \gamma_w\right)_{max} = \frac{1}{2}\left(\gamma_{w_{max}} - \gamma_{w_{min}}\right), \tag{7}$$

and Equation (4) becomes

$$S = \frac{g}{C_{L_{max}} U^2_{min}} \frac{\left(\gamma_{w_{max}} - \gamma_{w_{min}}\right)}{\bar{\gamma}_w} H \ . \tag{8}$$

Equation (6) is a requirement that the platform be neutrally buoyant for water at density $\bar{\gamma}_w$. As shown in Fig. 7, another way to state this requirement is

$$B_s = \bar{\gamma}_w H_s = W'_p + W_s \quad . \tag{9}$$

Note that H_s or W_s can always be adjusted to satisfy Equation (9) by using a buoyancy ballast or a weight ballast, respectively.

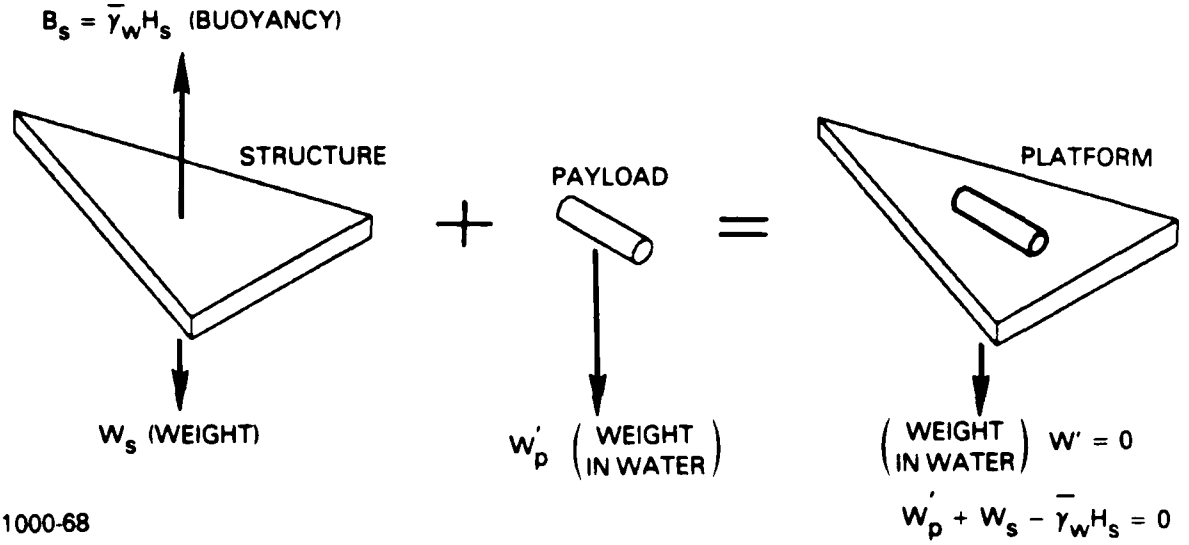

Figure 7. Relation Between Structural Volume, Structural Weight, and Payload Weight in Water for the Neutral Buoyancy Condition

3.4.2 Optimum Structural Volume and Payload Packaging Volume

The neutral buoyancy condition of Equation (9) can always be satisfied with the use of ballast or flotation. However, design integration can be used to minimize the total displaced volume while satisfying this condition. The payload weight is fixed, and it can be packaged in a sealed container of any size above a certain minimum. It is desirable to package it with this minimum volume. Minimum volume for payload packaging gives maximum weight in water for the payload. The buoyancy of the structure should just counteract this weight plus the weight of the structure itself (in air). By increasing this required buoyancy for the structure, the allowable volume of the structure

(without the use of ballast) is increased. Increasing the allowable structural volume gives a stronger wing and strength requirements are easier to satisfy.

3.4.3 Strength Requirements and Maximum Load Factor

Before proceeding, we need to consider the strength requirements for the wing. The maximum loads on the wing occur during the transition motion at the top and bottom of the traverse for maximum current operation. At the high current condition, the angle of attack during the transition will undoubtedly exceed the very small value required for normal lift. The situation is analogous to aircraft maneuvering for which high load factors occur. If we define the load factor as

$$n = \frac{L}{W'_{max}} \tag{10}$$

where W'_{max} is the maximum weight in water and is approximately given by

$$W'_{max} \simeq C_{L_{max}} \frac{1}{2} \rho_w U^2_{min} S \quad . \tag{11}$$

The load factor in the transition maneuver at maximum current is then

$$n_{man} = \frac{C_{L_{man}} \frac{1}{2} \rho_w U^2_{max} S}{C_{L_{max}} \frac{1}{2} \rho_w U^2_{min} S} = \frac{C_{L_{man}}}{C_{L_{max}}} \left(\frac{U_{max}}{U_{min}} \right)^2 \tag{12}$$

where $C_{L_{man}}$ is the lift coefficient during maneuver. Since

$$\frac{C_{L_{man}}}{C_{L_{max}}} < 1 \ , \tag{13}$$

the upper limit on the maneuver load factor is given by

$$n_{man} < \left(\frac{U_{max}}{U_{min}} \right)^2 \ . \tag{14}$$

The operating current speed range for the platform is large, so Equation (12) predicts very high maneuver load factors. On the other hand, the reference load, W'_{max}, for the load factor, is extremely small (the platform is "tuned" so that it never weighs very much in water).

3.4.4 Lower Limit on Size

The lower limit for the structural volume required for the buoyancy condition of Equation (9) occurs for zero structural weight, W_s. It is

$$H_{s_{min}} = \frac{W'_p}{\bar{\gamma}_w} \quad . \tag{15}$$

Thus, the lower limit on wing size is given by Equation (8) to be

$$S_{min} = \frac{g}{C_{L_{max}} U^2_{min}} \frac{\left(\gamma_{w_{max}} - \gamma_{w_{min}}\right)}{\bar{\gamma}_w} \left(H_p + \frac{W'_p}{\bar{\gamma}_w}\right) \tag{16}$$

3.4.5 Preliminary Design Using a Flat-Plate Wing Structure

In this section preliminary design calculations are made for a very simple wing construction, namely a flat plate. This type of construction is inexpensive but is not as efficient structurally as a shape with more thickness at the wing root. One purpose of this exercise is to determine whether the flat-plate type is adequate structurally when a sandwich construction is utilized. Another purpose is to obtain an estimate of the size of the wing.

The payload characteristics are taken to be as follows (see Section 2.2):

$$W_p = 55.0 \text{ N } (5.61 \text{ kg})$$

$$H_p = 2560 \text{ cm}^3 \quad .$$

This implies that

$$W'_p = 29.85 \text{ N} \quad .$$

The assumed envelope of water density is shown in Fig. 1, from which we obtain

$$\frac{\gamma_{w_{max}} - \gamma_{w_{min}}}{\bar{\gamma}_w} = 0.5 \times 10^{-2} = \frac{1}{2} \% \tag{17}$$

where we have used this relation between the change in σ and the change in γ:

$$\Delta\sigma \simeq \frac{\Delta\gamma_w}{\bar{\gamma}_w} \quad . \tag{18}$$

We take the minimum operating current to be

$$U_{min} = 3 \text{ cm/s}$$

and use

$$C_{L_{max}} = 1.0 \quad .$$

This is a conservative value for $C_{L_{max}}$. (Wentz, 1968, gives $C_L = 1.17$ for the wing we are using at an angle of attack of 30°.)

The first estimate in the iterative procedure for obtaining the wing area is obtained by using Equation (16), which assumes zero structural weight. The result is

$$S = 3054 \text{ cm}^2 \quad .$$

The structural weight (i.e., the weight of the wing) can now be estimated. Use the approximation given by Equation (15) to obtain

$$H_s = 3041 \text{ cm}^2$$

so that the wing thickness is

$$t = \frac{H_s}{S} = 0.996 \text{ cm} \quad .$$

Assume the following construction for the wing sandwich. The core is 192 kg/m^3 closed cell foam and the skins are fiberglass impregnated with resin with a density of 0.41 kg/m^2.* Given the preceding wing volume and wing area, the weights of the core and the skins are

$$W_{core} = 5.729 \text{ N}$$

$$W_{skin} = 2.44 \text{ N}$$

---

*These densities correspond to a core of 12 lb/ft^3 and a skin with 6 oz/yd^2 fiberglass cloth impregnated with an equal weight of resin.

so that the wing weight is

$$W_s = 8.17 \text{ N} \quad .$$

The wing volume is revised according to Equation (9):

$$H_s = \frac{W_p' + W_s}{\bar{\gamma}_w} \tag{19}$$

$$= 3874 \text{ cm}^3$$

which leads to a revised value for wing area according to Equation (8) of

$$S = 3509 \text{ cm}^2 \quad ,$$

a revised value for wing thickness of

$$t = \frac{H_s}{S} = 1.10 \text{ cm} \quad ,$$

and a revised value for total volume of

$$H = 6436 \text{ cm}^3 \quad .$$

For the approximate calculations being made here, iteration until convergence is not necessary. Thus, we stop at the current size estimate for the wing and we go on to consider the structural adequacy of the wing. For this consideration we assume the current will never exceed (see Section 2.3)

$$U = U_{max} = 60 \text{ cm/s} \quad .$$

Then the upper limit on the load factor according to Equation (14) is

$$n = \frac{L_{max}}{W'_{max}} \leq \left(\frac{U_{max}}{U_{min}}\right)^2 = 400 \quad . \tag{20}$$

The weight in water upon which the load factor is based is given by

$$W'_{max} = \left(\gamma_h - \gamma_w\right)_{max} H = \frac{1}{2} \frac{\left(\gamma_{w_{max}} - \gamma_{w_{min}}\right)}{\bar{\gamma}_w} \bar{\gamma}_w H \tag{21}$$

where Equation (7) has been used. Using previously obtained values yields

$$W'_{max} = 0.158 \text{ N} \quad ,$$

so that the maximum lift on the wing is

$$L_{max} = n\, W'_{max} = 63 \text{ N} \quad .$$

The aspect ratio of the wing planform is

$$AR = 1 \quad .$$

Thus the wing span is

$$b = \sqrt{AR \cdot S} \qquad (22)$$

$$= 59.2 \text{ cm}$$

A 1-cm-thick foam fiberglass sandwich wing with a span of 60 cm is very robust. The load requirement of 63 N is so small that detailed structural analysis is not needed. The flat-plate wing is structurally adequate.

3.5 Design With Buoyancy Compensation

In this section we describe the buoyancy compensation concept, give examples of how the compensator can be constructed, give the optimum platform density variation with depth, and then do a preliminary design calculation.

3.5.1 The Buoyancy Compensation Concept

The idea of buoyancy compensation is to utilize the increase in pressure with depth to compress a part of the platform so that the reduction in volume will compensate for the increase in water density and result in less change in the buoyancy force. This compressible part can either be an integral part of the structure or an added component.

3.5.2 Types of Compensators and Their Design

If the compensator is a separate part added to control the volume with depth, it could be spring-loaded plunger, a bellows, or simply a piece of elastically compressible material. An important requirement for the compensator is consistent action over time. It must not absorb water or exhibit fatigue. Also, it is desirable that the increase in volume due to addition of the compensator be small.

Another possibility is to make some portion of the structure a compensator. This has the advantage that no volume need be added. The water density increases by only a fraction of a percent from top to bottom of the platform excursion. To compensate, the volume of the platform decreases by the same fraction. For the flat-plate wing construction described above, the entire wing is a candidate for the buoyancy compensator. Since its volume is of the order of one-half the total volume, then the required fractional volume change for the wing will be about twice that required for the entire platform. This is a very small fraction, which indeed it needs to be to make the concept feasible.

3.5.3 Preliminary Design Using a Buoyancy-Compensating Wing

In this section we enhance the design developed in Section 3.4.5 by making the wing a buoyancy compensator. The design will be based on the water density envelope shown in Fig. 1. Also shown in the figure is the platform density variation that we chose as the optimum. It minimizes the difference between platform density and possible water density. A linear variation of platform density with depth has been assumed. This linearity follows from assuming that the wing stress-strain is linear. From Fig. 1 we obtain the following approximate values. The maximum deviation of platform density from water density is given by

$$\frac{(\gamma_h - \gamma_w)_{max}}{\bar{\gamma}_w} \simeq 1 \times 10^{-3} , \tag{23}$$

and the maximum change in platform density is given by

$$\frac{\gamma_{h_{max}} - \gamma_{h_{min}}}{\bar{\gamma}_w} \simeq 4 \times 10^{-3} . \tag{24}$$

These design input values are representative of operation in the Arctic. Other values used below are the same as used for the preliminary design in Section 3.4.5.

The platform volume is to be determined by iteration, and we start with an initial estimate of

$$H = 6400 \text{ cm}^3$$

for which

$$H_s = H - H_p$$

$$= 3838 \text{ cm}^3 \quad .$$

Then Equations (4), (22) and (23) give this wing size:

$$S = 1396 \text{ cm}^2$$

$$b = 37.4 \text{ cm} \quad .$$

Using the same procedure as in Section 3.4.5, the wing weights are calculated to be

$$W_{core} = 7.23 \text{ N}$$

$$W_{skin} = 1.11 \text{ N}$$

$$W_s = 8.34 \text{ N} \quad .$$

Then Equation (19) gives

$$H_s = 3891 \text{ cm}^3$$

and

$$H = H_s + H_p = 6453 \text{ cm}^3 \quad ,$$

which is close enough to the first estimate to stop the iteration. The wing thickness is

$$t = \frac{H_s}{S} = 2.79 \text{ cm} \quad .$$

We now consider the compressibility requirements for the wing's foam core. The fractional change in platform structural volume required for the change in density given by Equation (24) is

$$\frac{\Delta H_s}{H_s} = \frac{H}{H_s} \frac{H_{max}/W - H_{min}/W}{H/W} \simeq \frac{H}{H_s} \frac{\gamma_{h_{max}} - \gamma_{h_{min}}}{\bar{\gamma}_w} \qquad (25)$$

$$= 6.634 \times 10^{-3} \quad .$$

Now the change in pressure for a 300-m dive is about 3000 kPa. To obtain the change in volume given by Equation (25) when subjected to this pressure, the core material must have a compressive modulus 2 orders of magnitude less than obtained by standard structural foams.

Making the wing a buoyancy compensator offers the possibility of reducing the wing area by more than one-half. Its feasibility depends upon the availability of a foam core with the appropriate compressibility and strength. Foams that are much more compressible than standard structural foams are also considerably weaker. The strength requirements for the core are very modest, and it is possible that an appropriate foam exists for the core material; however, we have not investigated this.

3.5.4 Preliminary Design with a Buoyancy Compensator

In this section we enhance the design developed in Section 3.4.5 by using a separate part for a buoyancy compensator. As indicated in Section 3.5.2, a small compensator is desirable to minimize the increase in total platform volume.

The change in volume required is approximately given from calculations in the preceding section:

$$\Delta H_c = 26 \text{ cm}^3 .$$

If we make the reasonable assumption that the average volume of the compensator is not more than an order of magnitude greater than this required change, that is,

$$\bar{H}_c < 260 \text{ cm}^3 << \bar{H} ,$$

then the contribution of the compensator to the total volume can be neglected for preliminary calculations. With this presumption the wing sizing is the same as for the preceding section. In other words, if a compensator is used whose volume decreases by at least 10% during a dive to the bottom of the cable, then the increase in the total volume of the platform due to the presence of the compensator is insignificant.

Since choice for the foam core need not be constrained by compressibility requirements, as is the case for the buoyancy-compensating wing, the core can be chosen for strength requirements alone. In fact, if a structural foam is

used, a 2.5-cm-thick, 35-cm-span wing will be sufficiently strong to withstand a 23-N lift without a fiberglass skin. However, a resin coating reinforced with very light fiberglass cloth (0.05 kg/m^2) would be desirable just to protect and seal the foam, and a recalculation accounting for this reduced skin weight gives these results for wing area, span, and thickness:

$$S = 1260 \text{ cm}^2$$

$$b = 35.5 \text{ cm}$$

$$t = 2.64 \text{ cm}$$

These preliminary calculations indicate that the use of a separate buoyancy compensator is superior to the use of the wing as a compensator and that an effort to find an appropriate foam for the latter is not warranted.

3.6 **Climbing/Diving Performance**

The climbing/diving performance is of interest per se. In addition, the relationship between vertical speed and current speed is useful as a "calibration curve" to obtain current speed from a vertical speed measurement. This relationship can be computed, if equilibrium is assumed (i.e., no acceleration), provided we know the lift curve (C_L versus α), and the drag polar (C_D versus C_L) for the hydrofoil and the coefficient of sliding friction for the cable slider bearing. This calculation will be an approximation since these characteristics are not known precisely. The form of the relationship is shown in Fig. 8 for the designs considered previously. Vertical speed is initiated at 3 cm/s current and approaches the asymptote:

$$\text{Vertical speed} = U \tan \theta = 0.58\ U, \text{ for } U = \infty \qquad (26)$$

for large current speeds, where θ is the pitch angle of the wing as determined by a mechanical stop and is taken to be 30° in Equation (26) and in Fig. 8. The asymptote applies for an angle of attack of zero and gives a good approximation above current speeds of 10 cm/s, for which the previous designs have an angle of attack of less than 3°.

The above description is for a wing stop angle of 30°. This angle was conservatively chosen to be slightly less than the angle for maximum lift. For the diamond delta, the maximum lift angle is 35°. At this angle, the maximum climb speed would be approximately 70% of the current velocity.

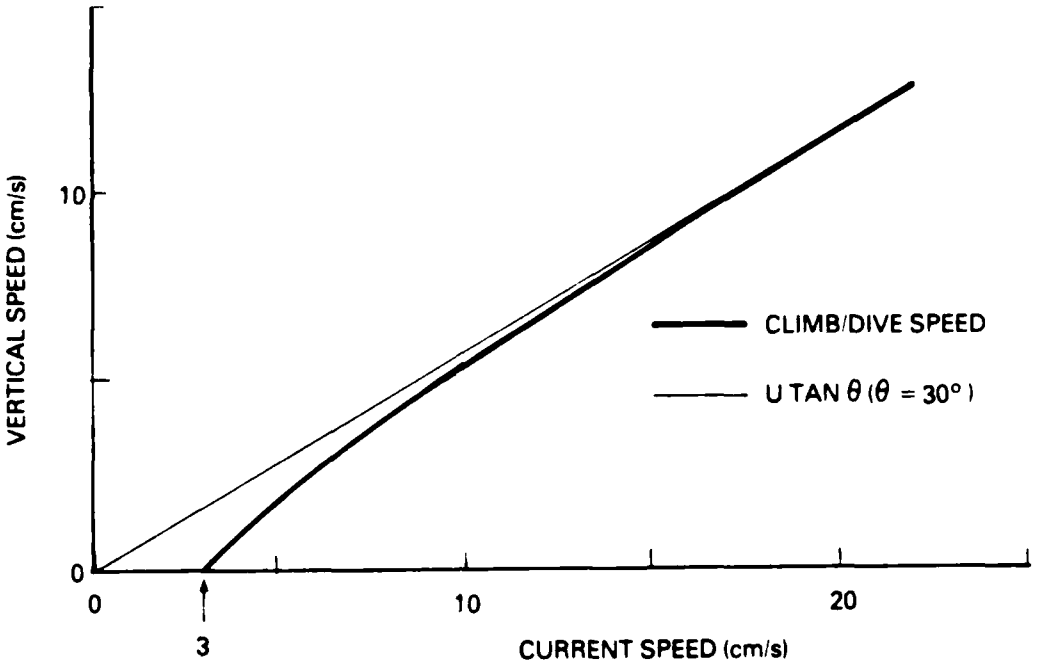

Figure 8. Climb/Dive Speed for a Wing Pitch of 30° and a 3 cm/s "Lift Off" Current Speed

To provide maximum performance at low current conditions (and produce the minimum current threshold velocity) the stop angle (maximum pitch angle) should correspond with the angle of maximum lift. As the vertical speed increases, the hydrofoil angle of attack decreases due to the relative velocity of the platform and the current. The vertical speed then is limited by this stop angle.

Higher ratios of climb speed to current speed can be achieved in two ways. If current speeds are high enough that the minimum threshold speed is not a concern, then the stop angle can be fixed higher than the angle of maximum lift. For example, a stop angle of 45° would produce a maximum vertical speed approximately equal to the current speed. The second way is to control the pitch angle actively. As the vertical velocity of the platform increases, the pitch angle would be made to increase to maintain an optimum angle of attack. This technique would produce platform speeds on the order of 2 to 4 times the

speed of the current. The disadvantage of this approach is the increased complexity and cost of the active pitch angle control system.

3.7 Control of the Platform Motion

Control of the vertical motion of the platform is obtained by controlling its pitch angle. Control of the pitch angle can be accomplished with an elevator either ahead (a canard) or behind (a tail) the wing or with flaps on the wing. In the following we will discuss power-actuated and passive control systems. The former is a control system for which the elevator or flap is driven by a power source in the platform (e.g., a battery-driven servo). For Arctic applications, the energy required for the considerable number of control actuations over a one-year operating period has to be stored on-board the platform or stored on the ice surface and transferred to the platform. A passive control system eliminates this power storage requirement. It is a control system that is driven by the external environment.

First, power-actuated controls will be addressed, then a mechanism that has been devised for passive control is explained. These explanations assume a canard elevator. For power-actuated control, a canard is desirable (as it is not affected by the considerable wake behind a delta wing) but is not essential; a tail or a wing flap could also be used. Also, an all-moving elevator is assumed. The entire control surface rotates. The hydrofoil must have up-down symmetry in addition to left-right symmetry. Thus, the elevator and the wing airfoil sections must be symmetric, and the center of pressure for each will be assumed to be fixed in the following analyses (see Appendix B). Also, unless otherwise stated, the analyses will be for the transition motion at the top of the cable.

In the following, reference to Appendix B will be helpful for understanding forces and moments on the system. One term, borrowed from aeronautics, may be unfamiliar to the reader. The neutral point, explained in detail in Appendix B, is a critical location point for the center of mass regarding pitch stability. If the center of mass is ahead of this point, the hydrofoil will be stable; if behind, it will be unstable. Also in the following we neglect moments about the center of mass due to the cable constraint forces. These in fact will be zero if the hinge point for the platform is at the center of mass.

3.7.1 Power-Actuated Control

Suppose the platform is configured such that the center of mass, the center of volume, the neutral point and the platform-to-cable hinge point all coincide. Then, according to Appendix B, any upward deflection of the canard elevator, however small, at any angle of attack will provide an upward pitching moment about the center of mass and, in the absence of a stop, the hydrofoil will diverge in pitch angle in the upward direction. The stop will then constrain the pitch angle to some maximum upward value (e.g., 30°), and the hydrofoil will home in on an equilibrium upward vertical velocity such that the net vertical force is zero. By using an all-moving elevator and hinging it at the center of pressure, the resisting hinge moment vanishes. Thus, changing upward to downward motion can theoretically be obtained with infinitesimal control deflection against infinitesimal resisting hinge moment resulting in infinitesimal power requirements. Finite deflections and power will be required in practice because of nonlinear hydrodynamic effects (the neutral point and the elevator center of pressure are not fixed points but move slightly) and because other considerations may not allow precise coincidence of the center of mass, center of volume, and hinge point. Careful design will make the energy requirement for control activation extremely small (at the control torque tube). Energy losses between the energy source and the torque tube and the considerable number of actuations per year will probably be the principal determinants of the energy storage requirements for an active control system.

Another aspect of the power-actuated control system that needs to be addressed is command of the elevator. What mechanism is to determine when the platform has reached the top or bottom of the cable and then command a reversal in elevator setting? Two techniques are suggested.

A depth (pressure) meter can be used to trigger the elevator at the maximum and minimum depths. Since depth is one of the conditions to be measured by the profiler, no additional sensing instrumentation would be required. Additional electronic hardware would be needed to create a command from the depth meter to the elevator driving mechanism. A schematic of such an elevator command and actuation system is shown in Fig. 9.

Another technique would be sensing something on the cable to trigger the elevator driving mechanism. The advantage of this method is that no on-board

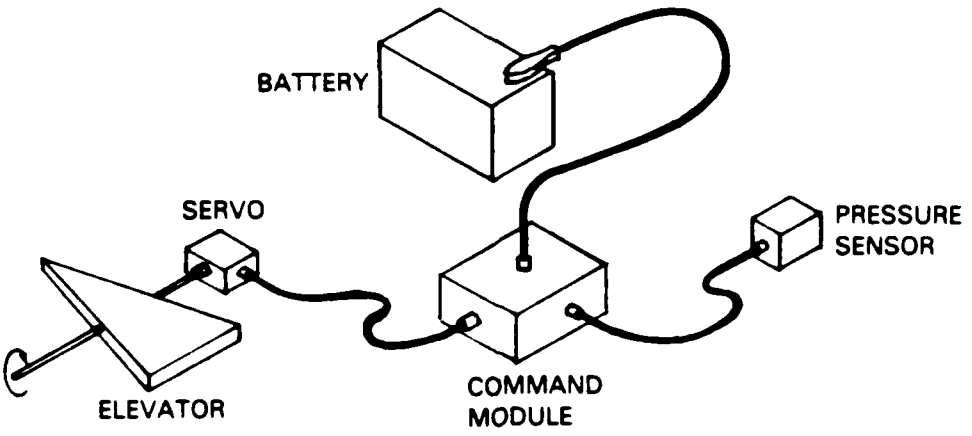

11000-71

Figure 9. Power-Actuated Elevator Control

monitoring of pressure sensor output would be required for the actuation. The potential problem of mechanical reliability could be reduced by using a magnetically operated, sealed switch.

3.7.2 Passive Control

To eliminate the need for a power source to drive the elevator, a passive control system has been devised and tested. It uses bumpers on the cable that cause platform nose-over when it is hit by the elevator of the rising (or falling) platform. It is appropriate first to describe a simpler system that was tried and failed. This system incorporated the most obvious way of using a cable bumper to cause nose-over. As illustrated in Fig. 10 a bumper contacts the nose of the platform at the top of the cable run. The upward momentum of the platform results in a nose-down rotation. The wing is loaded such that the center of mass is behind the center of pressure. Then the wing will be unstable in pitch, so once it experiences a positive or negative angle of attack, it will diverge in pitch until it hits the stop, which limits pitch excursion. The expectation is that at the top of the cable, a nose-down rotation sufficient to create a negative angle of attack will occur as shown in the sequence in Fig. 10.

Two problems occur with this scheme. First, if the mass of the platform is too small, the hydrodynamic damping will prevent it from executing a

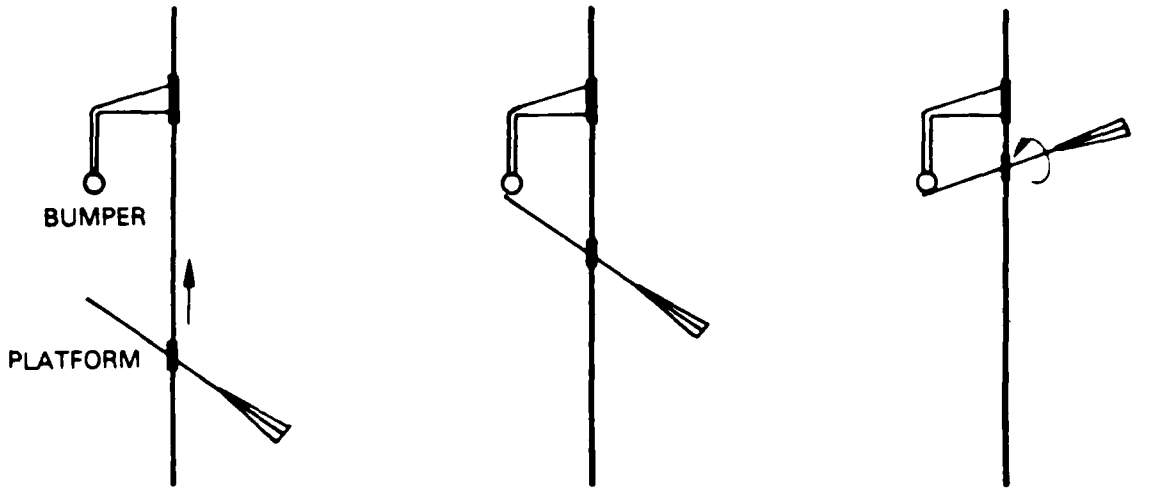

11000-72

Figure 10. Passive Control Scheme for Wing Alone

pitch-over. Instead, the platform will rotate about the bumper to an equilibrium pitch angle with no overshoot. This equilibrium pitch angle will be nose-up if the platform has positive weight in water. Increased upward velocity of the platform with attendant increased momentum for the nose-over does not help since hydrodynamic damping also increases and overshoot to negative angle of attack is still prevented. The experiments described in Section 4 verify this phenomenon.

The second problem with this scheme is that for positive weight in water, the platform will seek an equilibrium upward travel regardless of the initial condition. There is no possible equilibrium condition for downward motion. The resultant aerodynamic force necessary to counteract the downward weight in water cannot be generated without causing a flip-up of the wing away from its down stop. Thus, even if the platform makes the reversal of direction at the top, leaves the bumper, and travels downward, it will eventually stop and start moving up again because of the following sequence of events:

(1) With the platform held against the nose down stop by the negative lift, it accelerates downward until the vertical velocity is sufficient to cause a positive angle of attack.

(2) The platform rotates nose-up because of the lift direction reversal and continues to do so until it contacts the nose-up stop.
(3) The increasing lift eventually counteracts the weight in water, and the platform accelerates upward.

The problem of trying to rotate the entire wing with bumper action is alleviated by having the bumper serve merely to rotate an elevator, which is the basis of the passive control scheme that we successfully tested. The configuration is similar to that described for the power-actuated elevator. The difference is that bumper contact at the end of the excursion rather than power actuation causes a change in elevator setting. Other differences are that it is necessary to hinge the elevator behind its center of pressure, to have the center of mass slightly behind the center of pressure of the wing, and to have an elevator pitch excursion slightly larger than that for the wing.

The passive control scheme is best described in terms of the sequence of events that occur. Initially the platform is rising on the cable as shown in Fig. 11(a). In order for the canard to be held in the upward position, it is hinged behind its center of pressure. Thus the elevator is unstable in rotation and will always come to rest against its upper or lower stop and stay there depending upon its initial angle of attack. Also, in order for the wing to be held at its upward incidence position (25° for the platform shown in Fig. 11) during the upward traverse, it is necessary for the center of mass to be behind the neutral point. Thus the platform is unstable in pitch and will seek its upper or lower stop depending upon the initial condition.

When the bumper makes contact with the nose spike on the canard, it pushes it down. The canard rotates down about its hinge while the wing remains locked against its upward stop as shown in Fig. 11(b), (c) and (d). How and why this is accomplished is now explained.

By having the center of mass slightly behind the center of pressure of the wing, an even more severe requirement on the most forward center of mass position than established above, the lift on the wing will be sufficient to keep the wing locked in the upward position until the canard develops negative lift. Negative lift occurs after the bumper has pushed the elevator down to zero incidence [see Fig. 11(d)], that is, when

$$\theta_e = -\theta_w \quad . \tag{27}$$

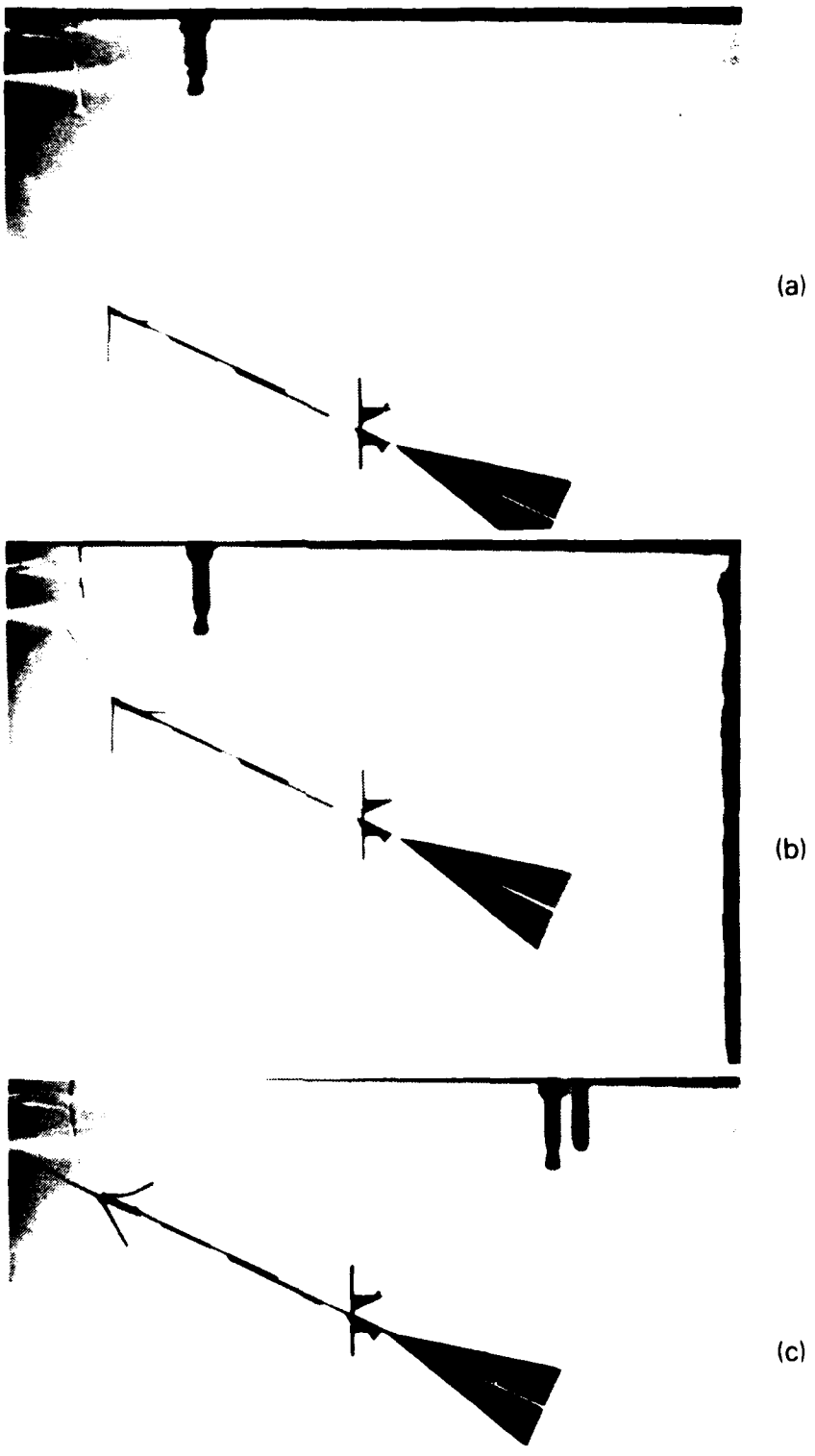

11001-07.1

Figure 11. Sequence of Events for Directional Change Using a Passively Controlled Canard

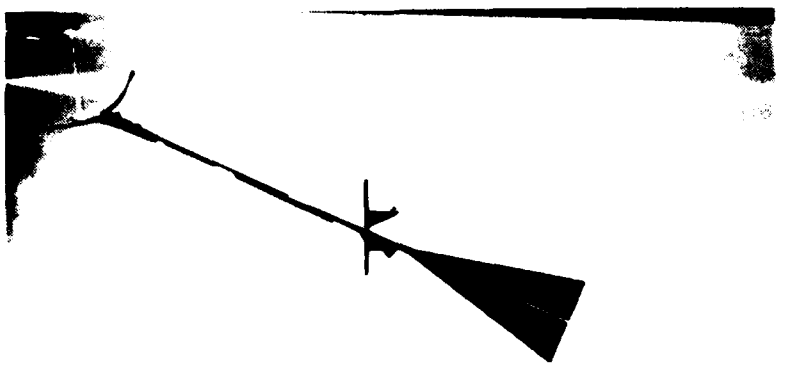

(d)

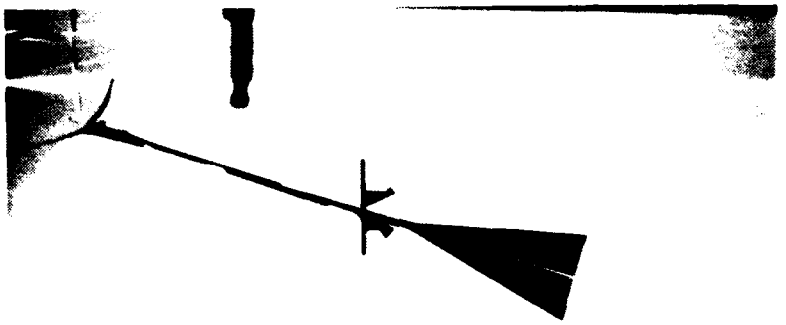

(e)

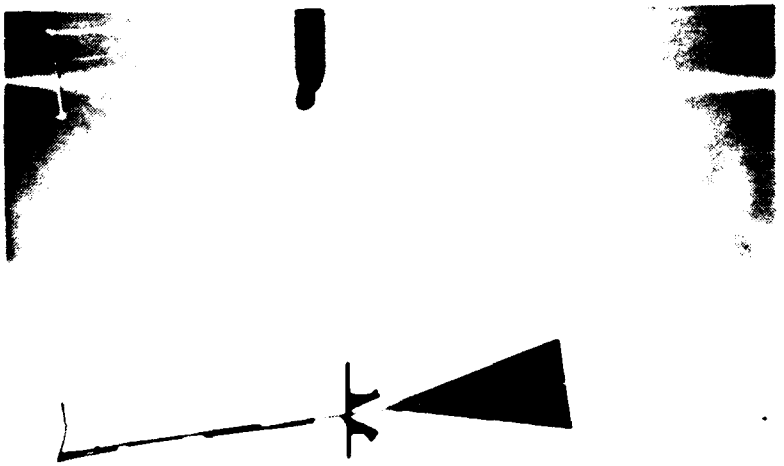

(f)

11001-07.2

Figure 11. Sequence of Events for Directional Change Using a Passively Controlled Canard (con't)

Thus it is necessary that the stops for elevator and wing rotation provide this inequality for the maximum excursions:

$$|\theta_{e_{max}}| \geq |\theta_{w_{max}}| \quad . \tag{26}$$

Next the platform rotates, nose down about its hinge when the canard develops sufficient negative lift as shown in Fig. 11(e) and (f). It is important that the canard experience negative lift before the platform rotates down, or else, as the platform rotates down, the elevator will rotate back up about its hinge to maintain contact with the bumper. As it leaves the bumper, the canard is locked into the down position and continues to develop more and more negative lift as the wing rotates down [see Fig. 11(e) and (f)] away from its upper stop. Reduction in wing lift with angle of attack results in downward acceleration of the center of mass, and the direction of travel is reversed.

It is necessary to consider what happens for downward travel when the weight in water is positive, that is, directed downward as we have been assuming. In particular we need to answer the question "Will the platform seek an equilibrium downward motion once started in that direction by interaction with the upper bumper?" Earlier in this section the wing-alone passive control scheme was shown to have no such long-term tendency to continue moving down. With the canard and with the above determined center of mass location and with elevator and wing stops needed for the passive motion reversal, equilibrium for downward motion does exist. The downward velocity increases until an angle of attack occurs such that there is equilibrium in vertical forces as illustrated in Fig. 12. It is necessary that the hydrodynamic moment about the center of mass be nose-down in order to maintain platform contact with the nose-down stop. The hydrodynamic force on the elevator supplies that moment. The stop supplies the constraint moment M_s needed for equilibrium in pitch (see Appendix B).

Since the platform rotates in yaw to face the variable current direction, contact with a bumper introduces some practical problems. The bumper can be allowed to rotate in yaw about the cable and can have a fin attached to it so that it too aligns with the current as shown in Fig. 13. An alternative is to use a ring bumper. For this option the diameter of the ring can be reduced by placing the cable closer to the canard. This setup requires an arm to

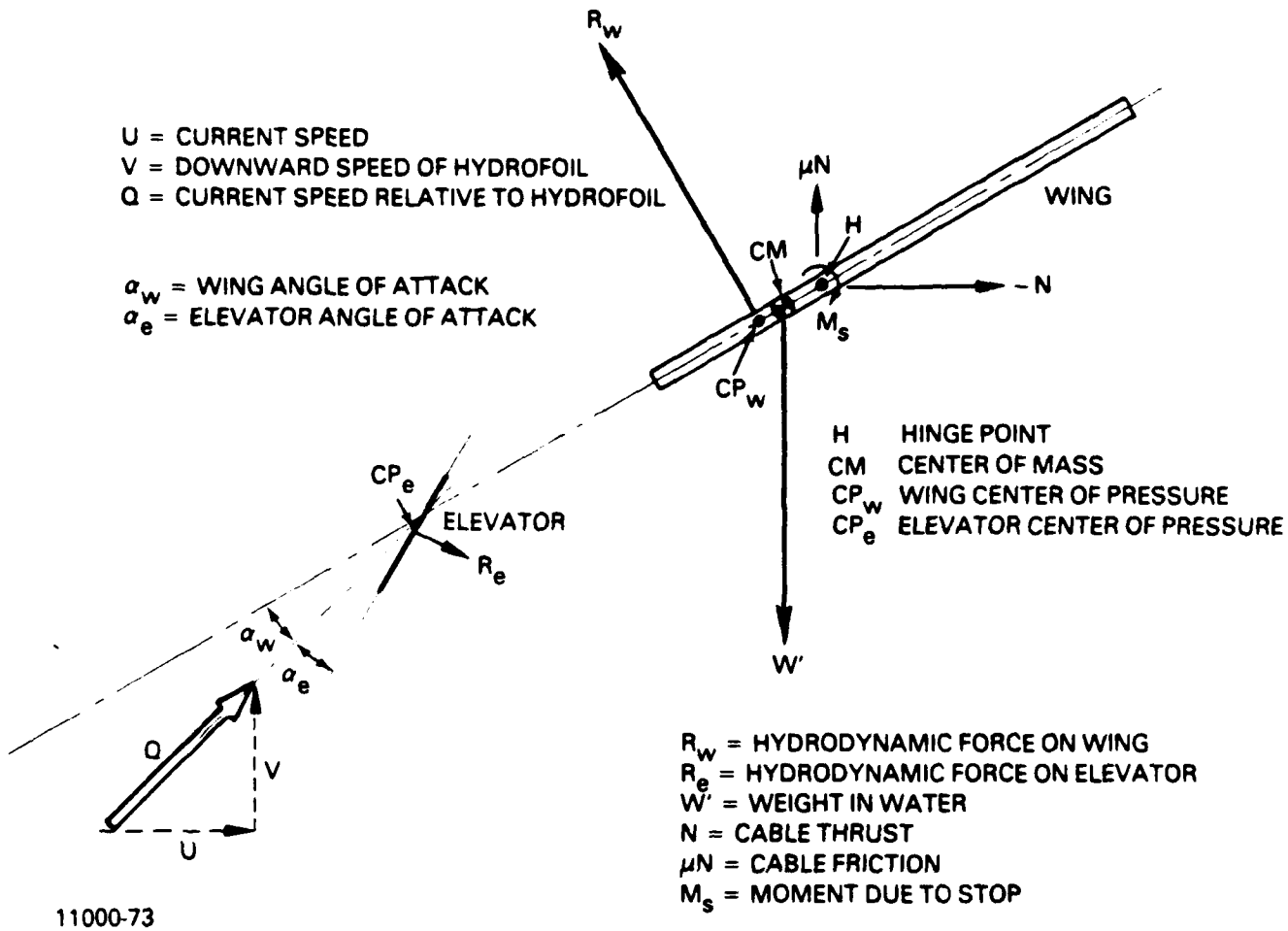

Figure 12. Equilibrium Condition for Motion in the Same Direction as the Weight in Water

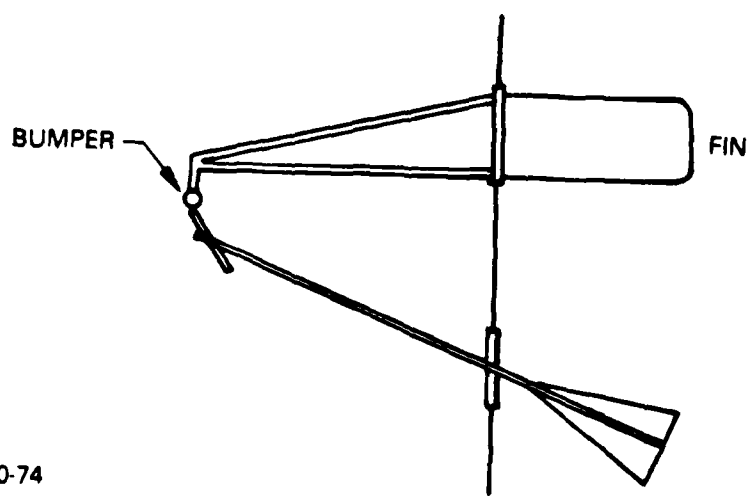

Figure 13. Finned Bumper

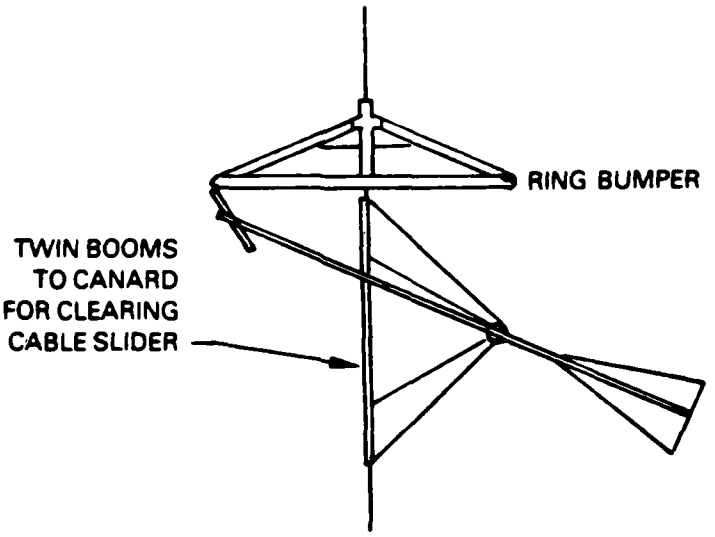

11000-76

Figure 14. Ring Bumper with Reduced Diameter Allowed by a Forward Cable Position

connect the cable slider to the pitch hinge as illustrated in Fig. 14. Note that twin booms are used to support the canard so that the cable can pass through just ahead of the wing without hitting any part of the platform. A third option is to locate the bumper close to the cable and to transmit the force through a control linkage (bell-cranks and a push-pull tube) to the canard. This reduces the necessary size of the bumper but increases the complexity of the control system.

3.7.3 Differences Between Passive and Active Control

Passive control requires the center of mass to be slightly behind the wing center of pressure. Active control requires the center of mass to be slightly behind the neutral point. For passive control large elevator excursions (e.g., $\pm 30°$) are needed. For active control only small elevator excursions are required (e.g., $\pm 5°$). For passive control the elevator is hinged behind its center of pressure, whereas for active control it is hinged on this point.

The disadvantages of active control are:

(1) Extra battery weight is required for storing energy for long-term operation.

(2) Additional hardware is necessary, including:

- o An electronic command module.
- o Control linkages and/or a sealed servo.

The disadvantages of passive control are:

(1) A bumper is required, which may be cumbersome to deploy through the ice.

(2) Bumper areas would increase the frontal area of the cable and would increase the wire angle of the cable.

(3) Under high current conditions, bumper impacts may fatigue and damage the control system or platform.

SECTION 4
TOW TANK TESTING OF HYDROFOIL PROFILER

4.1 Test Facility and Experimental Setup

An experimental investigation of the profiler using the yo-yo tethering scheme was conducted in the FLOW tow tank. This facility is described in Appendix C.

A weighted wire (solid stainless steel of diameter 0.05 cm) was towed through the tank. The platform was attached to the cable according to the yo-yo concept (see Section 2.4) as illustrated schematically in Fig. 15.

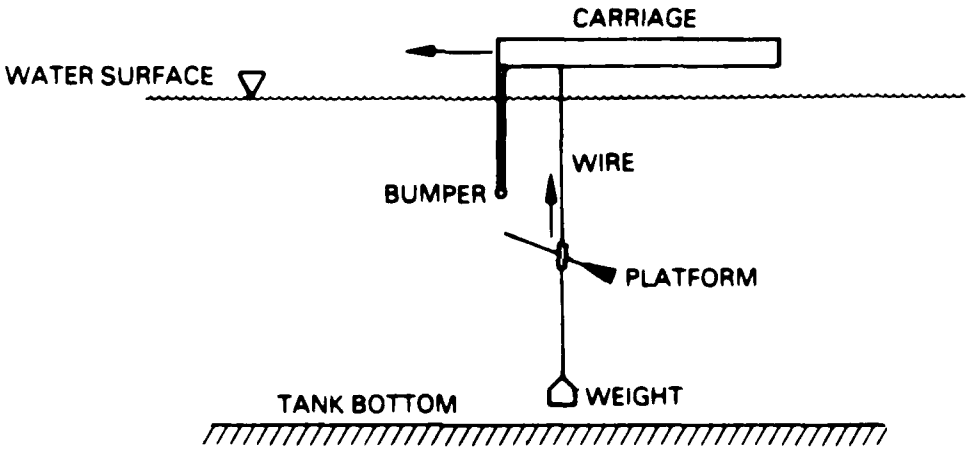

Figure 15. Tank Testing the Platform and Yo-Yo Concept

4.2 Purpose of the Tests

The vortex lift phenomenon for delta wings at high angles of attack has been thoroughly confirmed by extensive wind tunnel tests at Reynolds numbers several orders of magnitude greater than for the profiler operation. Test results show an insignificant effect of Reynolds number in going from wind tunnel tests to flight tests, but we have not been able to find any data for very low Reynolds numbers. Although a conventional wing's maximum lift would be reduced by about one-half at the operating Reynolds numbers for the profiler, this is not expected to occur for the delta wing. The leading edge separation phenomenon that creates the predominating vortex flow should be

independent of Reynolds number unless the Reynolds number is so low that the concept of a boundary layer no longer prevails. One purpose of the tests was to show that the maximum lift of a delta wing is not reduced at the low Reynolds numbers associated with profiler operation. Model 1 described in the next section was used for this purpose.

In addition to checking the hydrofoil's lifting performance, testing was done to assess the two schemes, discussed in Section 3.7.2, for travel reversal at the top and bottom of the cable. Models 1 and 2 described below were used for this purpose.

4.3 Description of the Models

Photographs of the models are shown in Figs. 16 and 17. Common features of both models are a vertical fin for directional stability, nearly all aluminum construction and a Teflon slide bearing at the vertical wire contact.

The first model, Model 1, is a wing alone with a planform as shown in Fig. 18. This planform is a modification to the basic delta and is called a diamond planform. The vertical fin is smaller than that shown in Fig. 18. The Model 1 fin is obtained by chopping off the fin shown in Fig. 18 (which was used for Model 2) at the wing trailing edge. The wing is a flat plate made from 0.17-cm-thick aluminum sheet. Aluminum pieces shown in Fig. 16 but not 18 were attached to the wing to increase the weight and to adjust the center of mass to a position shown in Fig. 18. This position is somewhat behind the center of pressure, for which the theoretically calculated location is also shown. The explanation for this center of mass requirement is given in Section 3.7.2. The model is of nearly uniform density; only the slider tube is not made of aluminum. Thus, the center of buoyancy and center of mass nearly coincide. Note that the hinge line and center of mass also nearly coincide. The model's mass is 62.5 gm, which corresponds to a weight in water of 0.395 N. Stops are placed in the cable slides to set the maximum wing incidence angle, θ_w, to $\pm 30°$ as indicated in Fig. 18.

The second model, Model 2, differs from Model 1 mainly by the addition of an all-moving elevator in the canard position as shown in Figs. 16 and 18. The wing is constructed from an aluminum plate with thickness of 0.084 cm. An additional plate, shown in Fig. 17, was attached near the nose for adjusting the center of mass to a location slightly behind the wing center of pressure,

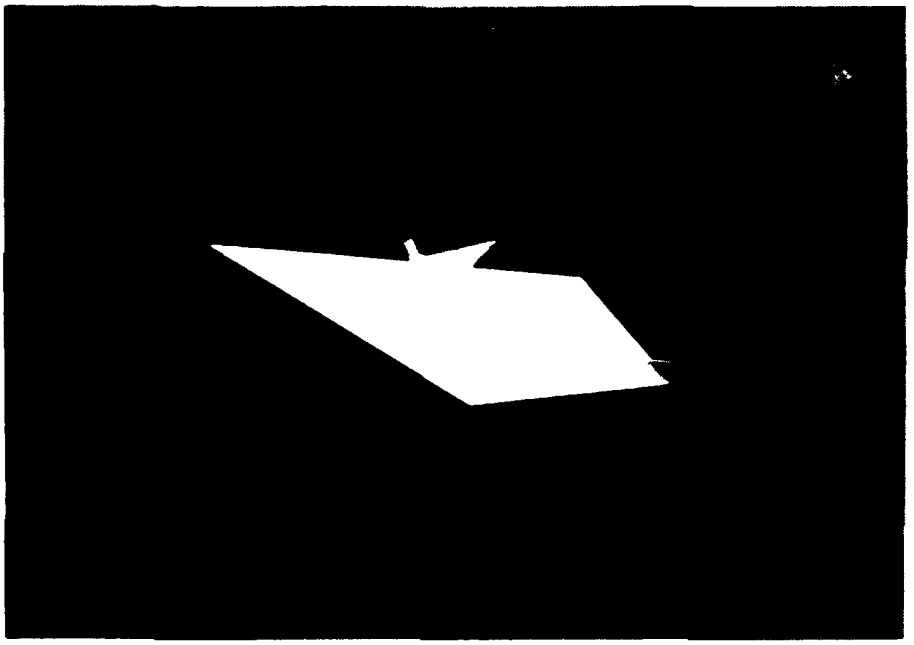

Figure 16. Model 1 - Wing Alone

11001-05

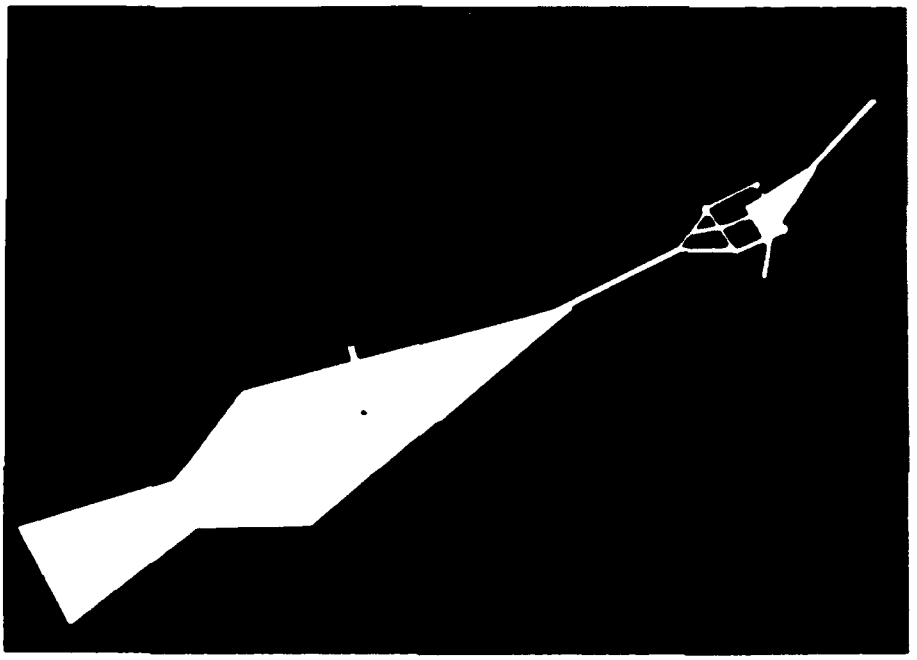

Figure 17. Model 2 - Wing and Canard

11001-06

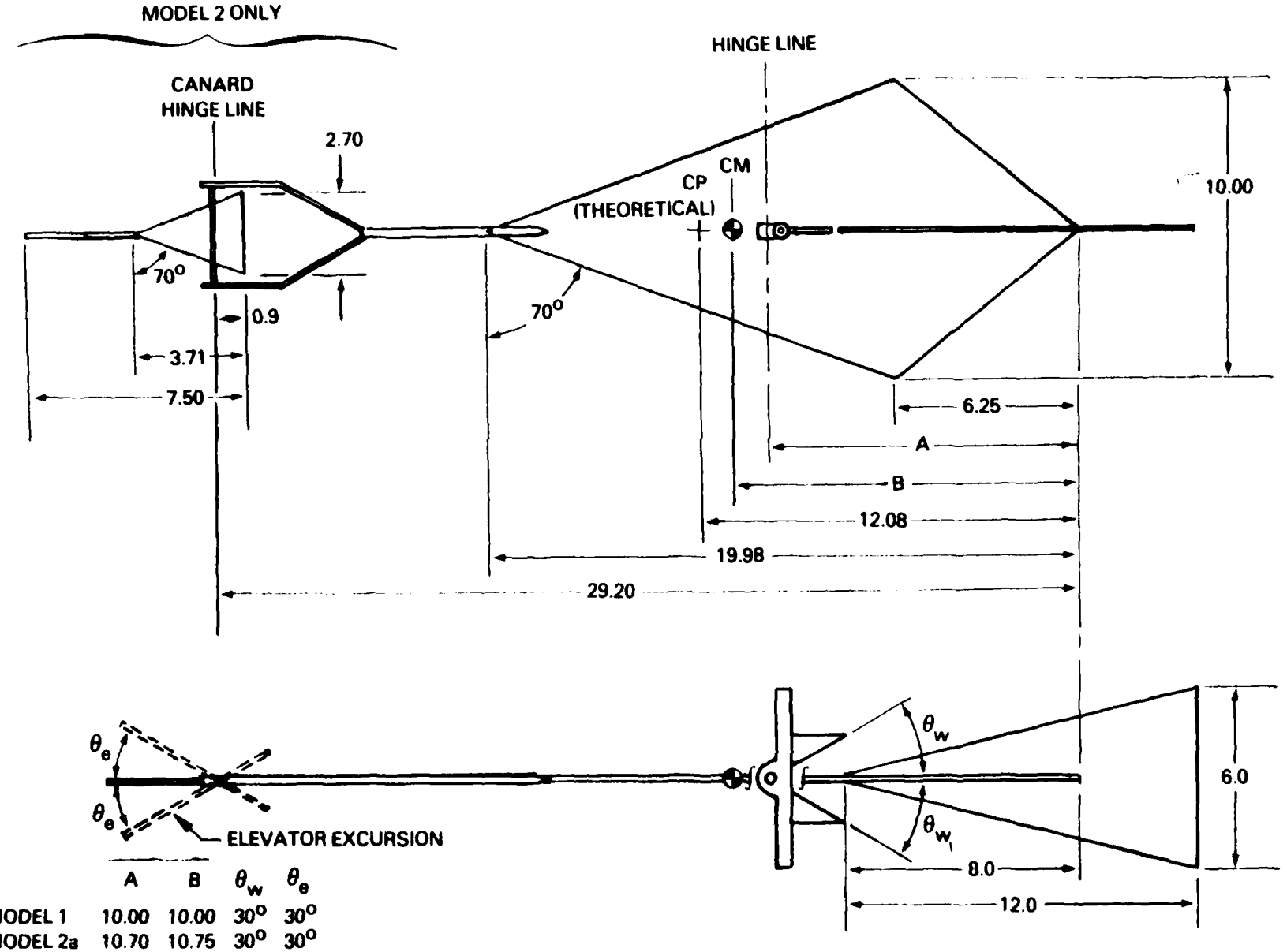

	A	B	θ_w	θ_e
MODEL 1	10.00	10.00	30°	30°
MODEL 2a	10.70	10.75	30°	30°
MODEL 2b	10.70	10.75	25°	35°

Figure 18. Model Dimensions (In Centimeters)

whose theoretical location is shown in Fig. 18. The explanation for this placement of the center of mass is given in Section 3.7.2. As for Model 1, the center of mass and the center of buoyancy are nearly coincident. Also, the hinge line is nearly on the center of mass as indicated in Fig. 18. The model mass is 37.7 gm, which corresponds to a weight in water of 0.238 N. Models 2a and 2b differ only in the stops used to set the rotational excursions of the wing with respect to the cable, θ_w, and of the elevator with respect to the wing, θ_e. As indicated in Fig. 18 these are $\pm 30°$ and $\pm 30°$ respectively for Model 2a and $\pm 25°$ and $\pm 35°$ respectively for Model 2b.

4.4 Lift Performance Test

A test was made with Model 1 to check the lifting performance at very low Reynolds numbers. These data were compared with the performance expected from theory.

Measurements - With the model set at 30° incidence, speed was gradually increased until the model just started to creep up the cable starting with a "stuck" condition where the static friction kept the model from climbing. Then the speed was reduced until the model again stopped on the wire and then reduced more until the model became "unstuck" and just started to move down. These two critical speeds were

$$U_{unstuck} = \begin{cases} 29 \text{ cm/s for upward motion} \\ 25 \text{ cm/s for downward motion} \end{cases} \tag{29}$$

Theory - For the first critical speed, the equation for vertical equilibrium gives (see Appendix B)

$$L = W' + \mu_s D \quad , \tag{30}$$

and for the second critical speed,

$$L = W' - \mu_s D \quad . \tag{31}$$

We can use these equations to calculate the critical speeds if we assume that the wing lift and drag correspond to those for wind tunnel tests from Wentz (1968). The calculations also require an assumption for the coefficient of friction. Fortunately, the influence of this parameter on the calculated speeds is weak.

To use the wind tunnel results we nondimensionalize Equations (30) and (31) to

$$\frac{W'}{\frac{1}{2}\rho_w U_{crit}^2 S} = C_L \pm \mu_s C_D \quad . \tag{32}$$

From the wind tunnel tests (Wentz, 1968, Figs. 5.16.1 and 5.16.2), we obtain at an angle of attack of 30°:

$$C_L = 1.16$$

$$C_D - C_{D_o} = 0.70$$

where

$$C_{D_o} = C_D \text{ at } C_L = 0 \quad . \tag{33}$$

We assume

$$C_{D_o} = 0.05$$

and

$$\mu_s = 0.15 \quad .$$

Fortunately the calculations are weakly affected by these assumptions. Thus using the weight in water, and wing area for Model 1, Equation (32) gives the following critical speeds:

$$U_{crit} = \begin{cases} 27.5 \text{ cm/s for upward motion} \\ 24.9 \text{ cm/s for downward motion} \end{cases} \tag{34}$$

It should be noted that the high "unstuck" speeds observed in the tank tests are not indicative of those for full-scale operation. The wing loading (i.e., the weight in water per unit wing area) for the tank tests was purposely made much higher than for the operational case in order to test at low Reynolds numbers. This resulted in the higher speeds for the tank tests. It is of interest to calculate the "unstuck" speed for the operational case directly from that observed in the tank. We need to assume dynamic similarity for

frictional and hydrodynamic forces. The latter implies a matching lift coefficient, from which it follows that

$$U_o = U_t \frac{b_t}{b_o} \left(\frac{W'_o}{W'_t} \right) \tag{35}$$

where the subscripts t and o imply tow tank and operational conditions, respectively. Thus calculation of the "unstuck" speed for upward motion for the design of Section 3.4.5, for which

$$W'_o = 0.158 \text{ N}$$

$$b_o = 59.2 \text{ cm}$$

with use of Model 1 characteristics, namely,

$$W'_t = 0.395 \text{ N}$$

$$b_t = 10 \text{ cm} \quad ,$$

gives

$$U_o = 3.1 \text{ cm/s} \quad .$$

This value is a very close match to the minimum operational current speed of 3 cm/s used as a design criteria in Section 3.4.5.

Conclusions - The agreement between Equations (29) and (34) and between Equation (35) and the design minimum speed used in Section 3 is quite good and supports the contention that the model is behaving according to the data obtained from wind tunnel tests. The lifting performance has not been significantly degraded by the reduction in Reynolds number from the value of about 10^6 (based on mean aerodynamic chord) for the wind tunnel tests to the value of 2.5×10^3 for the tow tank tests. The operating Reynolds number for minimum velocity for the full-scale platform will be of the order of 10^3, the same order of magnitude as for the tow tank tests.

4.5 **Travel Reversal Tests**

Tests were conducted with both models to test out the strategies for travel reversal discussed in Section 3.7.2.

Tests Without an Elevator - With Model 1 it was discovered that the technique described in Section 3.7.2 for travel reversal for a wing alone is not feasible. With a tow speed of 30 cm/s, for which the model was very slowly traversing up the wire, the model hit the bumper and stopped quickly without nose-over. Increasing the speed did not improve the situation. The model came to an equilibrium rest condition well above zero incidence even when it hit the bumper with much higher vertical velocity. Increasing speed did not appear to change significantly the nose-up stopping position. The increased momentum available for nose-over was not adequate to overcome the increased damping.

Tests With a Canard Elevator - Model 2, the model with the all-moving canard elevator, was tested to check out the second strategy for motion reversal described in Section 3.7.2. Some of the results have already been described and presented in that section and in Fig. 11. Those results are for Model 2b. A measure of the transition time is the time the model remains in contact with the bumper. From the video recordings made of the test, this time was determined to be 2.12 seconds with a tow speed of 30 cm/s. Although the transition still occurred for Model 2a it was much slower. The bumper contact time was measured to be 5.16 seconds at the same tow speed. This indicates the desirability of making the excursion for the elevator rotation larger than that for the wing.

A video of the tests made with Models 2a and 2b is part of the documentation for Phase I.*

Conclusions - For a passive travel reversal scheme using a bumper mounted on the cable, it is necessary to have the bumper actuate an elevator rather than attempt to rotate the hydrofoil directly.

4.6 Directional Stability Observations

The fin on Model 1 was less than half the size of that for Model 2 but, nevertheless, was observed to provide adequate directional stability.

*A copy of this video is available from FLOW's Laboratory Video Library and another copy is being supplied with this final report.

SECTION 5
A PROTOTYPE PROFILING SYSTEM

The prototype autonomous oceanographic profiler (AOP) presented in this section is a preliminary design based on the analyses, tests, and design calculations reported in the preceding sections. This design is a feasible solution to the oceanographic data acquisition capability to be obtained by the AOP system. Although this specification is not rigidly fixed for the future development of the profiler, the final prototype is not expected to differ greatly from the following definition.

The sensors on the proposed platform (see Fig. 19) are for temperature, conductivity and pressure (depth). The current speed can be approximately calculated from the vertical velocity of the platform, as measured by the rate of change of pressure. Therefore, the AOP, even if not equipped with a direct-current meter, will provide profiles of current speed via calculation by an on-board computer. A low-cost compass could be added to obtain current direction.

The platform configuration, a delta wing with a canard elevator, is described in Section 5.1. Data sampling, its telemetering to satellites, and power requirements for this function are described in Section 5.2. The power budget is discussed in Section 5.3, and the vertical cable is described in Section 5.4. Antifouling provisions are specified in Section 5.5, and cost estimates for the entire system are given in Section 5.6. Finally, in Section 5.7, non-Arctic applications for the AOP system are discussed.

5.1 Hydrofoil Design

The wing planform will be a diamond planform with a 70° leading-edge sweep as defined in Fig. 18. In order to operate in currents as low as 3 cm/s with the instrument payload of 5.6 kg, buoyancy compensation is used and the wing span is conservatively set at 45 cm. The corresponding platform length is 140 cm. The wing thickness will be 2.54 cm. A hard plastic resin coating reinforced with light fiberglass cloth (0.07 kg/m^2) will protect a closed-cell, high-density (200 kg/m^3) foam core. The vertical fin will be half the size (relative to the wing) of that shown in Fig. 18 and will not extend beyond the wing trailing edge (see Fig. 19).

A buoyancy compensator will be used. It will be constructed of a moderately compressible material to provide a volume reduction of about

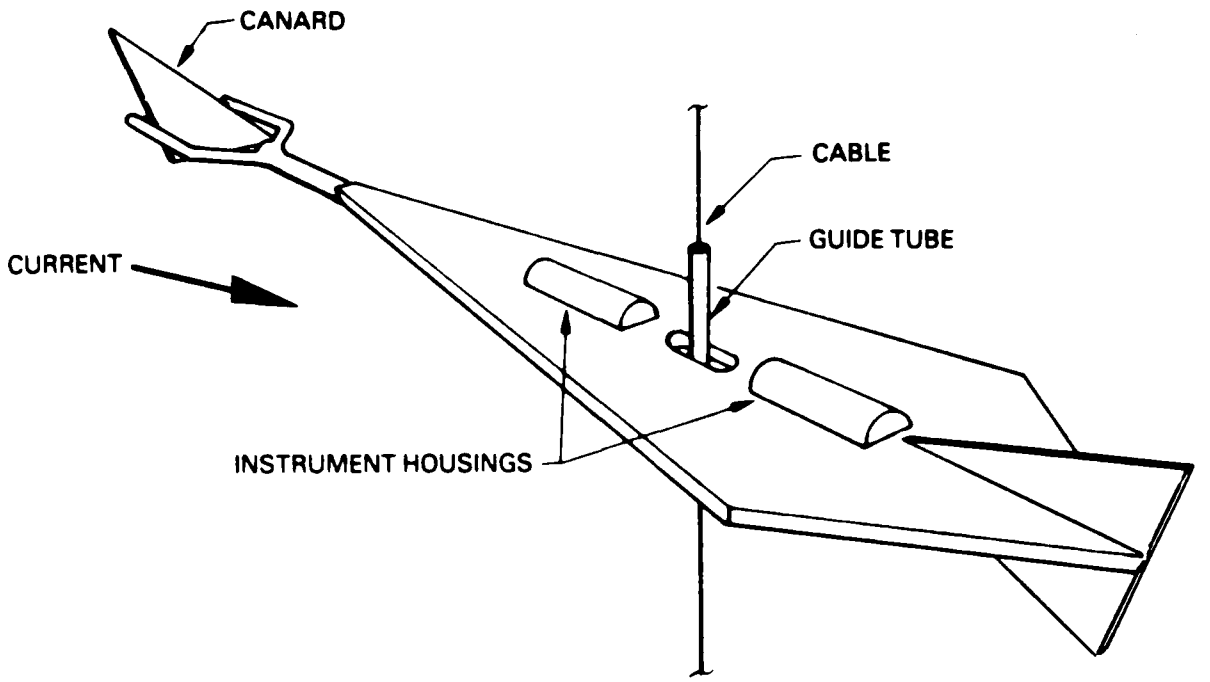

11000-83A

Figure 19. Proposed Prototype Platform Configuration

30 cm^3 with a dive to 300 m and will have a relaxed volume not exceeding 300 cm^3.

The hydrofoil will use a canard elevator for pitch control. The system that is the current choice for reversing the hydrofoil motion at the top and bottom of the cable utilizes a bumper, attached to the cable, which actuates the elevator upon contact. Since the hydrofoil can swing in any direction to point into the current, we plan to use a ring bumper and thus cover all possible positions of the canard elevator. Although this solution is feasible and has been tested, other bumper concepts may be preferable. Additional investigation on rotating finned bumpers and on small ring bumpers that contact an actuator located nearer the cable is warranted. For the latter, a mechanical linkage between the actuator and the elevator is required.

Although current choice is for a passive control system as described above, our study of an active elevator control system showed that power requirements

are feasible. The advantages provided by this control system are significant, especially for non-Arctic applications. Therefore, development of an active control system is also warranted.

5.2 Sampling and Telemetry Design

As discussed in Section 2.1, the design sampling rate should be 4 casts per day to 300 m with 2-m resolution or 600 data points per day for temperature, conductivity, depth and time. These samples must be taken at the platform, transmitted to the surface buoy and then through ARGOS. The goal is to keep the system as inexpensive, reliable, and long lived as possible. This dictates that the electronics design be simple with the trade-off that regular, high-frequency sampling is not required. In keeping with simplicity of design, it is desirable to avoid transmitting power or signals through the cable between the surface buoy and the moving platform. The present design calls for internally powering the platform and transmitting the data to the surface with a low-power acoustic link similar to that found in Aanderaa RCM-4 current meters.

In an effort to keep the system simple, the sampling may be carried out on a timed sample basis. That is, the temperature, conductivity and depth sensors would be sampled every 2.4 minutes resulting in 600 samples every day, enough for four separate profiles of 150 2-m sample bins each. If the platform is cycling rapidly, these may be made over many more than four actual profiles. If the currents are weak and the instrument is not cycling, a time series at a fixed depth may be produced. For a typical ice velocity of 7 cm/s and a vertical profiling speed of 3.5 cm/s during one day, the platform will accumulate four profiles worth of data over five up/down cycles of the platform to 300 m. This scheme uses the simplest sampling control software but requires a somewhat complicated analysis scheme. It also may provide interesting internal wave data during periods of no vertical motion.

A sampling scheme that may require less power in the platform and that might make analysis more straightforward at the expense of increased platform software complexity would be to continuously sample pressure only and then to sample temperature and conductivity only if pressure had changed to correspond to a new depth bin. If the continuous pressure sampling interval remained 2.4 minutes, then the maximum number of samples would remain unchanged and, for the 3.5 cm/s vertical velocity, samples would be obtained every 5 m of travel.

Using all five up and down casts would still yield an average of 4 samples per 2-m bin.

With either scheme, data will have to be transmitted from a buffer in the platform to the ARGOS transmitter. The simplest approach would be to transmit the last 150 samples taken each time the platform reaches the surface. This will require approximately 2 minutes over a 300-baud acoustic link. For vertical speeds greater than 2.8 cm/s, 150 samples will cover all samples, and for vertical speeds between 2.8 and 1.4 cm/s, all of the samples from the previous up cast will be recovered. For vertical speeds less than 1.4 cm/s, some of the samples from the bottom of the previous up cast and all from the previous downcast will be lost.

The buoy electronics at the surface will have to listen continually for the acoustic transmission from the platform, store the incoming samples in a buffer, and continuously transmit the buffer contents through ARGOS. If the platform collects a sample every 2.4 minutes and the buoy transmits at least 4 samples every minute, each sample will be transmitted through ARGOS an average of 9.6 times before being replaced. With one satellite in view for 10 minutes once very 101 minutes, 10% of the transmissions get through. Any one sample will have a 96% chance of getting through. With two satellites, each sample will get through an average of 1.92 times. Given this situation, the surface buoy electronics buffer should be of the first-in/first-out type but perhaps should require that each sample be transmitted 10 times before replacement. The platform electronics should only transmit to the surface buoy as much new data as was acquired in the previous up/down cycle and, of course, no more than 150 samples should be transmitted to the surface buoy.

5.3 Power Budget and Endurance

As currently envisioned, the platform and surface buoy will each have their own autonomous electrical system. The platform will be powered by its own internal battery pack and will transmit data to the surface buoy via a low-power acoustic link when it is near the surface. Thus, there are separate power budgets for the platform and the hull.

There are four basic components in the platform that require power: the pressure, temperature, and conductivity sensors, and the controller. The controller maintains the sampling schedule, stores data, and transmits the data

through the low-power acoustic link to the surface buoy. The power requirements of these components are as follows:

- Controller, 3 mA @ 12 V in quiescent mode
  10 mA @ 12 V when sampling/transmitting
- Pressure sensor, 1 mA @ 12 V (Paroscientific)
- Temperature sensor, 10 mA @ 12 V (Sea-Bird, SBE-3)
- Conductivity sensor, 10 mA @ 12 V (Sea-Bird, SBE-4)

The sampling scheme is that the controller will remain on continuously and will turn on the sensors once every 2.4 minutes. Continuous controller operation will require a cumulative current drain of 3 mA for one year or 26.3 A-hr per year at 12 V.

The sensors must be sampled for 2.0 seconds every 2.4 minutes. During sampling, a total of 31 mA is required. Six hundred samples per day will require 0.01 A-hr/day or 3.8 A-hr/year, again at 12 V. The total power requirement is then 30.1 A-hr at 12 V for one year. This can be supplied by three battery packs, with four lithium D cells per pack. Such a battery supply will require a space 6.8 x 6.8 x 18.3 cm (2.7 x 2.7 x 7.2 in.) or 846 cm^3 (52.5 in^3) and would weigh 1.36 kg (3.0 lb).

The surface buoy electronics would be very similar to existing Polar Research Laboratory (PRL) buoy designs. These designs, which incorporate a controlling microprocessor, transmitter and atmospheric pressure and temperature measurements, draw an average of 11 mA or 96.4 A-hr/year at 12 V minimum. These needs can be met by seven standard PRL alkaline battery packs, each 20.3 cm in diameter by 6.1 cm thick (8-in. diameter x 2.4-in. thick).

5.4 Cable

The cable upon which the platform moves vertically should have several qualities. Given that it will support an end weight of 100 to 200 lb, it must have a safe working load on the order of 500 lb. To avoid adding excessively to the surface buoy buoyancy requirements, it must not be unduly heavy. Perhaps most important, the coefficient of friction between it and the instrument must

be quite low. Finally, it must be possible to deploy the cable without powered equipment and undue complications.

Several possibilities have been considered for the appropriate combination of the slider mechanism on the platform and the cable. The two most likely candidates are: (1) a Teflon sliding fixture with a solid stainless-steel wire and (2) a Teflon- or polypropylene-jacketed galvanized-steel wire with a stainless-steel sliding fixture. The first concept has the advantages of very low sliding friction and low cost. The disadvantages are that all wear occurs on a small area of the sliding fixture, making it prone to failure, the corrosion resistance of the bare wire is questionable, and the solid wire would be difficult to deploy. The second candidate would be relatively easy to deploy, and the wearing surface would be spread over the whole cable. With a Teflon jacket, the cost might be high, but if a polypropylene jacket can be used without creating too great a friction penalty, the cost would be reasonable.

For the present, it is assumed that the cable will be polypropylene-jacketed, 1/16-inch, galvanized-steel cable 300 m long. It will weight about 10 lb, cost about $300.00 and support a safe working load of approximately 500 lb. The slider fixture will be a smooth stainless-steel cylinder. At present, it is assumed that a roller-type fixture will not be used but, if the friction of the slider appears to be too high, the added complexity of a roller fixture will be worth the price.

5.5 **Marine Fouling and Corrosion**

For extended deployments, bio-fouling and corrosion may degrade the performance of the AOP system or even disable it if they cause sufficient changes in the density of the platform. We anticipate using proper caution in selecting combinations of different metals for the profiler as one means of reducing corrosion due to electrolytic effects. We also recommend using one of the many commercially available antifouling coatings both to protect the corrodable surfaces and to retard the attachment and growth of marine organisms and vegetation on the platform. These coatings include antifouling paints, one type of antifouling wax (Aqua-Tek), and an antibiotic marine paint additive ("Compound X"). Many of these coatings are copper-based and toxic to the environment. Recently, newer antifouling paints have been developed that do not exhibit strong toxicity over long periods and may be useful where environ-

mental considerations are important. We do not foresee requiring any new technology to address the potential fouling and corrosion problems.

5.6 Estimated Cost of System

The estimated cost of the AOP system, detailed by subsystem, is given below. For this costing, the system is equipped with sensors for temperature, conductivity and pressure.

Subsystem	Cost
Surface Buoy Electronics and Hull. Includes ARGOS Transmitter	$ 6,200
Surface Buoy Acoustic Interface and Transducer	$ 2,500
Temperature, Conductivity, and Pressure Sensors, Related Hardware, and Underwater Housing	$ 8,500
Acoustic Interface, Transmitter, and Transducer in Platform	$ 3,000
Guide Cable and Hardware	$ 1,500
Platform and Control Surface	$ 2,900
TOTAL ESTIMATED COST	$24,600

This estimate was developed with input from Polar Research Laboratory of Santa Barbara, California, and from Sea-Bird Electronics of Seattle, Washington. All of the electronics and sensor systems are either commercial products or adaptations of existing commercial equipment, which serves to reduce development costs and the cost of components for individual buoys.

The cost of a SALARGOS-type buoy, equipped with six pairs of sensors, is $50,000. Therefore, the proposed AOP system will not only provide greater vertical resolution than present technology but also will provide it at approximately one-half the overall cost.

5.7 Non-Arctic Applications

The proposed prototype AOP described above is targeted for Arctic drifting buoy applications. The profiler could also be configured for non-Arctic data gathering in a number of applications. The surface area of the hydrofoil

would be tailored to the current magnitudes expected in a given area and to the desired vertical speed of the platform. As the proposed wing shape is simple and the wing materia: is inexpensive, it would be convenient and low-cost to interchange wings of different surface areas.

One configuration would be as an expendable drifting buoy suspended from a surface float. Unlike a string of sensors suspended from a surface float, the platform would be decoupled from the vertical wave motion; as the surface float is lifted, the cable would pass through the guide tube without imparting vertical motion to the platform. Differential current velocity, required to drive the platform vertically, would be obtained by having a drogue at a depth away from the depth range being profiled. For example, if the surface waters were to be profiled, a drogue would be suspended from the bottom weight of the cable to a depth well beyond the influence of surface currents. If deep profiling were desired, then the surface float would provide the differential motion.

Another application would be for near-shore monitoring on the continental shelf. Here the AOP could be bottom-anchored with a near-surface float. A number of data recording and data recovery methods are possible. The data could be internally recorded and recovered when the platform is recovered. The data could be stored in the platform and acoustically transmitted to a surface vessel upon command. A third method would be to transmit acoustically the data to a surface float, which then would transmit the data via satellite.

The AOP system will not be able to monitor internal waves in the same manner that a string of conductivity and temperature sensors can monitor such phenomena. The vertical velocity of the platform is simply not high enough to provide unambiguous data except for very low frequency waves. However, the platform could monitor internal waves in a more direct manner. Using an active vertical control system, the platform could be programmed to identify the region of maximum density variation and then to follow this isopycnal surface as internal waves pass. This would be analogous to the way in which a Waverider Buoy measures surface waves. In this case, the height and period of the wave would be derived from the pressure sensor output.

SECTION 6
CONCLUSIONS

The conclusions of this feasibility study are given below.

- The use of a hydrofoil platform to obtain profiles of ocean properties over long deployment periods is quite feasible.

- Through tow tank testing it was determined that the maximum lift of the delta-type wing is independent of Reynolds number down to values as low as 2,500. This is in contrast to the approximately 50% reduction in maximum lift expected to occur for a rectangular wing at these Reynolds numbers.

- Because of its high lift performance at low Reynolds numbers and the low span for a given wing area, a highly swept delta wing configuration is most appropriate for the hydrofoil profiler.

- The use of a passive direction reversal system (that is, one requiring no power source other than provided by the ocean current itself) is both feasible and practical.

- The most severe test of the hydrofoil profiler concept is in regions of low current velocity, such as in the Arctic Ocean. Even for currents as low as 3 cm/s, a profiler of physically reasonable dimensions will be able to produce vertical motion from the currents. Operation can be obtained at even lower currents with a larger hydrofoil area or less deviation from neutral buoyancy.

- For optimal performance in low current regimes, buoyancy compensation is necessary. That is, the displaced volume of the profiler must be reduced at depth to compensate for the increased water density.

- The hydrofoil profiler will provide greater vertical resolution at lower cost than existing data gathering systems.

REFERENCES

Coachman, L. K., and Aagaard, K. (1974) "Physical Oceanography of Arctic and Subarctic Seas," in Marine Geology and Oceanography of the Arctic Seas, Y. Herman, editor, Springer-Verlag, New York, pp. 1-72.

Katz, E. J., and Nowak, R. T. (1973) "A Towing System for a Sensing Package: Experience and Plans," Journal of Marine Research, 31, 63-76.

Morison, J. H., and Smith, J. D. (1981) "Seasonal Variations in the Upper Arctic Ocean as Observed at T-3," Geophysical Research Letters, 8(7), 753-756.

Morison, J., Burke, S., Steltner, H., and Andersen, R. (1982) "SALARGOS Temperature-Conductivity Buoys," Oceans, September, 1255-1260.

Van Lee, J. C. (1976) "An Automatic Oceanographic Profiling Instrument," ISA ASI 7626B, 489-500.

Wentz, W. H. Jr. (1968) "Wind-Tunnel Investigations of Vortex Breakdown on Slender Sharp-Edged Wings," NASA CR-98737, November.

Wingham, P. J. (1983) "Comparative Steady State Towing Performance of Bare and Faired Cable Systems," Ocean Engineering, 10, 1-32.

APPENDIX A
EVALUATION OF KITE CONFIGURATION

A.1 Analysis of the Kite Configuration

Two different tether/profiler configurations were considered for achieving the stated sampling goals. One of the concepts we examined was that of a lifting surface tethered in a flow by a conducting cable. Resembling a kite on a string extending downward from a top tether on an ice floe in the Arctic, the profiling platform could ascend and descend in the water column by changing its angle of attack in the flow. For other applications, tethering could either be to the bottom or at mid-depth on a fixed-point taut-wire mooring.

As a first step in evaluating the feasibility of the kite configuration, computer codes were written to model the equilibrium shape of the tether cable in a horizontal flow. Modeling consisted of two components: one that described the hydrodynamic characteristics of the platform, and one that used those data along with cable and flow parameters to predict the equilibrium shape of the cable in terms of vertical and horizontal displacements with distance along the cable. We made calculations for both bare and faired cable cases.

The basic goal of the computer simulations was to determine whether or not the kite could achieve desired vertical excursions (continuous sampling between 5 and 300 m depths) under a range of flow conditions (0.05 to 0.60 m/s). We assumed a top tether with 600 m of cable, as might be used in the Arctic, and a mid-depth tether with a cable length of 100 m, as might be used in continental shelf applications.

To initiate the analysis, a current speed and the angle of the tether cable relative to horizontal at the platform are input to the computer program, which describes the hydrodynamic characteristics of the platform. This program calculates the tension at the platform end of the cable due to the lift (positive or negative) generated by the platform in the current. These values of tension and angle are then supplied to a second program, which determines the equilibrium shape of the cable itself. Vertical and horizontal platform excursions as a function of length along the cable are calculated from the equilibrium shape of the cable.

Cable angles are measured positive upward from horizontal. Thus, a positive initial cable/platform angle places the platform below the tether point. In

comparison, a negative cable angle places the platform above the tether point under ideal conditions, although such is not always the case. Fig. 2 shows simple examples of different cable/platform geometries.

It may be helpful to keep in mind that the tension/angle specifications at the end of the cable represent a fixed boundary condition and that the cable calculations are static in nature. Thus, the cable shape program determines the unique equilibrium shape of the cable necessary to fulfill the fixed cable end conditions with a given set of cable parameters. For these analyses, the maximum cable/platform angle is $\pm 60°$. An angle of 60° was considered a physically reasonable maximum value upon which to base initial calculations. Also, larger angles would require that the platform generate greater tension in the tether cable, increasing the size and structural requirements of the wing. Finally, the kite performance becomes questionable only at low current speeds, and, in this case, the cable angle decreases rapidly with distance from the platform and becomes shallow over most of the cable length. Thus, increasing the cable/platform angle would make little difference at higher speeds and would have little effect at low speeds. An angle of +60° is expected to result in the platform being below the level of the tether. Given a set of cable parameters, the cable shape program predicts just what that distance below would be. With a given set of input parameters, if the cable program predicted an equilibrium shape that placed the platform 250 m below the tether when the goal was picked as 300 m, then the kite could not meet the desired performance specifications for this particular case.

A variety of cases were examined in which different combinations of speed, cable weight, bare or faired cable, and initial cable angle with respect to the platform were used. The basic question to be answered was simple: for a given cable weight and reasonable total cable length, could the kite achieve equilibrium cable shapes that (1) placed the platform near the surface and (2) placed the platform at or below the target depth of 300 m if flow speeds were between 0.05 and 0.60 m/s? This could be cast another way: could the platform in one flight configuration (i.e., angle of attack) generate enough lift to carry one end of the cable to the surface, and in a second configuration, could the platform generate enough downward force to pull the cable end to 300 m or deeper in spite of the opposition stemming from drag forces on the platform and cable?

Based upon specifications for commercial cables that met the projected strength and conductor requirements, a cable diameter of 0.4 cm was chosen. The corresponding weight in water is 0.1461 N/m (for reference, 1 lb/1000 ft = 0.0146 N/m). A maximum cable length of 600 m was chosen because a longer cable would be more susceptible to tangling and because of generally shallow cable angles near the tether in low-tension conditions, a longer cable would not yield appreciable differences in achieved depth. The following cases were examined in the order given here: (1) bare cable, nominal weight in water equal to 0.1461 N/m; (2) bare cable, neutrally buoyant; (3) bare cable, slightly negatively buoyant, 0.0005 N/m; and (4) faired cable, 0.0146 N/m. The values of 0.0005 and 0.0146 N/m were determined by calculating the change in cable weight that would result from a seawater density change of 0.4%. Calculations were made for current speeds of 0.05, 0.10, 0.30, and 0.60 m/s. Table A-1 summarizes the results of the computer analysis of the kite concept.

Table A-1. Summary of Kite Configuration Analyses - Table values are vertical excursions (in meters) of the platform relative to the tether point (refer to Fig. 2 for illustration of positive and negative angles and excursions). Total cable length = 600 m.

			Bare Cable			Faired Cable	
			WPUL (N/m)				
Speed (m/s)	Angle (degrees)	Tension (N)	0.0000	0.0005	0.1461	0.0000	0.0146
0.05	-60	1.11	+270	+229	-580	>368	-438
0.05	+60	1.44	-304	-332	-599	<-404	-575
0.10	-60	5.85	+306	+299	-570	>315	+85
0.10	+60	5.84	-306	-313	-590	<-394	-507
0.30	-60	55.53	+313	-312	-23	>395	+377
0.30	+60	52.31	-306	-306	-328	<-405	-420
0.60	-60	223.21	+314	-314	+249	>401	+391
0.60	+60	209.08	-305	-306	-359	<-404	-410

In the case of a bare cable with a weight in water of 0.1461 N/m, the platform could easily achieve a depth of 300 m or greater below the tether point at all speeds. The cable weight aided greatly in achieving deep descent. At speeds of 0.10 m/s and less, the cable dangled almost vertically. However, only for a speed of 0.60 m/s could the platform achieve a depth either equal to or above that of the tether point. In this case, the cable weight greatly hindered the shallow performance of the kite. Thus, at low current speeds, it would be impossible for the kite to sample the upper part of the water column if the cable had a nominal weight in water, and this particular platform/cable configuration does not constitute a feasible approach to fulfilling the performance goals.

Using a perfectly neutrally buoyant bare cable, the platform could achieve both the deep and shallow target depths. For all speeds, the equilibrium depths were about the same distance, slightly greater than 300 m, above and below the tether point. In the Arctic and nearly any other marine locale, however, both temporal and spatial (particularly in the vertical) variations occur in the seawater density. This means that the effective weight in water of the cable (and platform) changes, and therefore deviations occur from the ideal, neutrally buoyant conditions. In practical terms, a particular cable/platform configuration that performs satisfactorily at one location or season may not do so at another location or season.

Assuming a maximum variation of 0.4% in the density of seawater yields an effective change of 0.0005 N/m in the cable weight in water. The kite analysis was performed using this value for the weight of the cable. For speeds of 0.10 m/s and greater, there is little difference between the results for this case and those for the perfectly neutrally buoyant cable case. For a speed of 0.05 m/s, the platform descended deeper than at the greater speeds or for the neutrally buoyant case. However, the platform ascended a smaller distance above the tether than for the neutrally buoyant case. For a bare cable weight in water of 0.0005 N/m, the kite concept could satisfy the performance goals of the project. Subsequent analysis showed that the cable weight in water would need to reach 0.0025 N/m before the bare cable kite could not reach the shallowest sampling depth for a current speed of 0.05 m/s.

For the sake of completeness, cases were analyzed using a faired cable rather than a bare cable. Faired cables have less drag than comparably sized

bare cables (roughly 30% as great). The rationale was that better performance might allow using a shorter cable with the attendant advantages of decreased cable cost and decreased danger of tangling. As expected, the faired cable performance exceeded that of the bare cable for the neutrally buoyant cable case for all speeds. However, since fairing increases the cross-sectional area over that of the basic bare cable, changes in seawater density cause correspondingly greater changes of faired cable weight in water. The change in faired cable weight in water is 0.0146 N/m, assuming a 0.4% change in seawater density. At speeds of 0.30 m/s and greater, the faired cable performance bettered that of the bare cable. At a speed of 0.10 m/s, the deep faired cable performance was better than that of the bare cable, but while still acceptable, the shallow faired cable performance was worse than that of the bare cable. At a speed of 0.05 m/s, the faired cable could not achieve the shallow performance goal, although it easily achieved the deep. Thus, using a faired cable did not provide a viable approach to increasing the level of performance of the kite concept.

So far, we have presented only the results of analyses intended to determine whether or not the kite concept could physically achieve the earlier-stated sampling goals of the profiling system. It can. However, there are other considerations that have to be taken into account before finally settling on the most promising concept. Other considerations of the kite concept that led us to pass it over in favor of the yo-yo concept are as follows: One immediate problem is that of achieving nearly exact neutral buoyancy of the cable. Even small changes in cable weight in water strongly affect performance, so that starting with a neutrally buoyant cable is a strict necessity. This is difficult to ensure. Also, should a cable be even slightly compressible, then the effective weight in water would change as the cable ascended and descended, again a condition that would be difficult to compensate for.

Because drag and cable weight are important factors in determining the depth range of the platform, the kite is effectively limited in terms of the depth range that it can sample. Unless cable tension is very high, cable angles tend to get shallow, on the order of 10-20°, near the tether. In this situation, adding to the length of the cable not only fails to increase the depth range by much, but also increases the cost by about a dollar a foot of cable.

Another consideration that is difficult to assess is the problem of tangling of the cable, particularly in the transition from quiescent to higher current conditions. A kink in the cable could well lead to conductor failure with time.

For reliable operation, the kite needs active controls for reversing the vertical direction of travel. With proper design, this may be only a minor detail, but it does require more power and adds somewhat to the complexity. In fairness, it should be mentioned that, while the yo-yo is the more amenable to entirely passive controls, it also may employ active controls, and so the complexity and power needs are a consideration for that application also.

There is also a need for a very reliable slip-ring arrangement, probably near the top of the cable or perhaps in the electronics housing resting on the ice (or somehow out of the water). The reason is oceanographic in nature. Currents tend to have a rotary nature primarily because of the tides. Thus, a kite in a semi-diurnal tidal regime would execute two revolutions about the tether point every 24 hours. With no provision to allow the cable connection to rotate, the cable would twist. For short deployments, this may not be a problem, but over longer deployments (which are one goal of this program), the unrelieved twisting could lead to kinking and conductor failure or to alterations in the roll attitude of the platform.

To meet the sampling performance goals, it is necessary to fly the platform at an angle of attack that generates relatively large values of lift. At a current speed of 0.60 m/s, the cable tension is over 200 N or roughly 50 lb, and the platform and tethering yoke must have the structural integrity to withstand the stress. Since force is proportional to the square of the speed, higher speeds would generate appreciably higher stresses on the mechanical structure.

There are some practical problems associated with faired cables. Fairings increase the cost of the cable, and make deployment a much more complicated process, an important detail when working under harsh conditions. Also, fairing sections may suffer "shake-off" over a deployment, leading to the degradation of performance. We conclude that fairings should not be used for a kite-type profiler.

The considerations detailed above are in the context of a surface tethered Arctic application. The kite may be quite acceptable for use in shallower

applications, perhaps with a mid-depth tether. A much shorter cable could be used, lessening cable drag and the possibility of tangling. While the platform might require reinforcement to withstand the higher current speeds, it would generate greater lift, so that performance would be affected to a smaller degree by seawater density changes. The cable twisting problem would still need to be addressed.

A.2 Description of Computer Codes

Details of the computer programs that were developed to describe the hydrodynamic performance of a delta wing shape and to calculate equilibrium cable shapes for the kite profiler concept are presented below. Included is a presentation of the force balances and an outline of the operation of each program.

Considerations of size, simplicity, and method of lift generation pointed toward a delta wing shape for the platform. The basic details of delta wing performance were drawn from existing literature and incorporated into a computer program. Given inputs of the current speed and cable angle at the platform, the program determined the magnitude of the tension in the cable produced by the upward or downward hydrodynamic force generated by the platform. These cable angle and tension values, along with other inputs, were used by a second program, which then determined the unique equilibrium shape of the cable for this particular set of inputs. Vertical and horizontal excursions relative to the tether point were then calculated as functions of length along the cable. Magnitudes of the vertical excursions were then examined to determine whether or not the respective configurations could meet the profiler's performance goals.

A.3 Analysis of the Wing Hydrodynamic Performance

Fig. A-1 portrays the force balance on a tethered lifting surface. Under equilibrium conditions, the sums of the horizontal forces and of the vertical forces are zero. The forces are lift, drag, cable tension, and the weight in water. The latter is the sum of the gravitational and buoyancy forces on the platform. Both lift and drag depend upon the angle of attack and therefore are functionally related to each other. This functional relationship is termed the drag polar and depends upon the particular wing design. NASA document CR-98737 (Wentz, 1968) was used to obtain the drag polar for our particular choice of

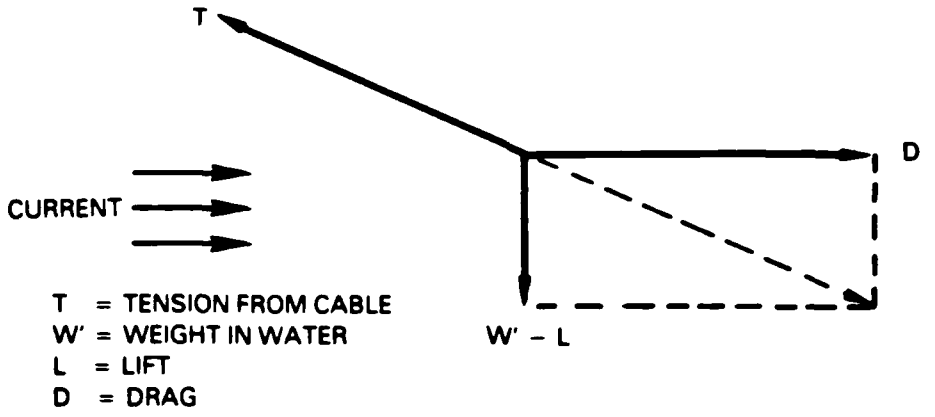

11000-80

Figure A-1. Forces Acting on an Underwater Kite — An equilibrium condition is shown as an example. It does not necessarily represent the true relationship among magnitudes under actual conditions.

delta wing shape. The force balance equations are

$$\text{Vertical forces:} \quad L + T \sin \beta = W' \tag{A.1}$$

$$\text{Horizontal forces:} \quad D = T \cos \beta. \tag{A.2}$$

By definition,

$$D = C_D \, q \, S \tag{A.3}$$

and

$$L = C_L \, q \, S \, , \tag{A.4}$$

where

$$q = 1/2 \, \rho_{sw} U^2 \, . \tag{A.5}$$

Here, L is the lift, D is the drag, T is the cable tension, W' is the weight in water of the platform, C_D and C_L are the coefficients of drag and lift, respectively, S is the area of the wing, β is the angle between the platform and cable, q is the dynamic pressure, ρ_{sw} is the density of seawater, and U is the current speed.

The equations yield the relation

$$F = L/D + \tan \beta - W'/D = 0 \quad . \tag{A.6}$$

Recall that each of the variables is defined in terms of C_L, so that Equation (A.6) can be satisfied by the proper choice of C_L.

The computer program solves the problem using the following sequence of operations:

(1) Given ß, ρ_{sw}, U, and the drag polar, construct a table of C_L and corresponding values of F.

(2) Find the value(s) of C_L for which F = 0. There may be two values.

(3) For this value(s) of C_L, find the corresponding value(s) of C_D from the drag polar.

(4) Calculate T = D/cos ß.

Thus, the program yields the cable tension which, combined with the hydrodynamic forces acting on the wing, produces a balance of both horizontal and vertical forces. Dual values of C_L mean that the wing can fly at two different angles of attack, each of which yields tension values that satisfy the set of force balance equations. For these analyses, the larger tension value was chosen when two values were possible. The results of the hydrodynamic force analysis were then used as input for the cable shape program.

A.4 Analysis of Tether Cable Shape in a Uniform Current

Fig. A-2 shows a sketch of the forces acting on a cable segment in a flow. A uniform flow in the vertical was assumed.

Simple balance equations may be written for both the vertical and horizontal forces:

$$\text{Vertical forces:} \quad T \sin ß + (\Delta W' - \Delta L) = (T + \Delta T) \sin (ß + \Delta ß) \qquad (A.7)$$

$$\text{Horizontal forces:} \quad T \cos ß + \Delta D = (T + \Delta T) \cos (ß + \Delta ß). \qquad (A.8)$$

Here, T is the cable tension, ΔD is the drag on the cable segment, $\Delta W'$ is the weight of the cable segment in water, ΔL is the lift on the cable segment, and ß is the angle between the cable and horizontal at the platform. These equations can just as easily be written in terms of normal and tangential forces on the

cable, and the results of the analysis will be identical. Indeed, just such a formulation was used in the faired cable analyses.

Solving for values of ΔT and $\Delta \beta$ using the equations given above yields:

$$\Delta T = \Delta D \cos \beta + (\Delta W' - \Delta L) \sin \beta \qquad (A.9)$$

and

$$\Delta \beta = [(\Delta W' - \Delta L) \cos \beta - \Delta D \sin \beta] (T + \Delta T). \qquad (A.10)$$

For the force equations above, the drag and lift were obtained from the following equations:

$$\Delta D = q\, d\, C_D\, \Delta \ell \qquad (A.11)$$

and

$$\Delta L = q\, d\, C_L\, \Delta \ell \ , \qquad (A.12)$$

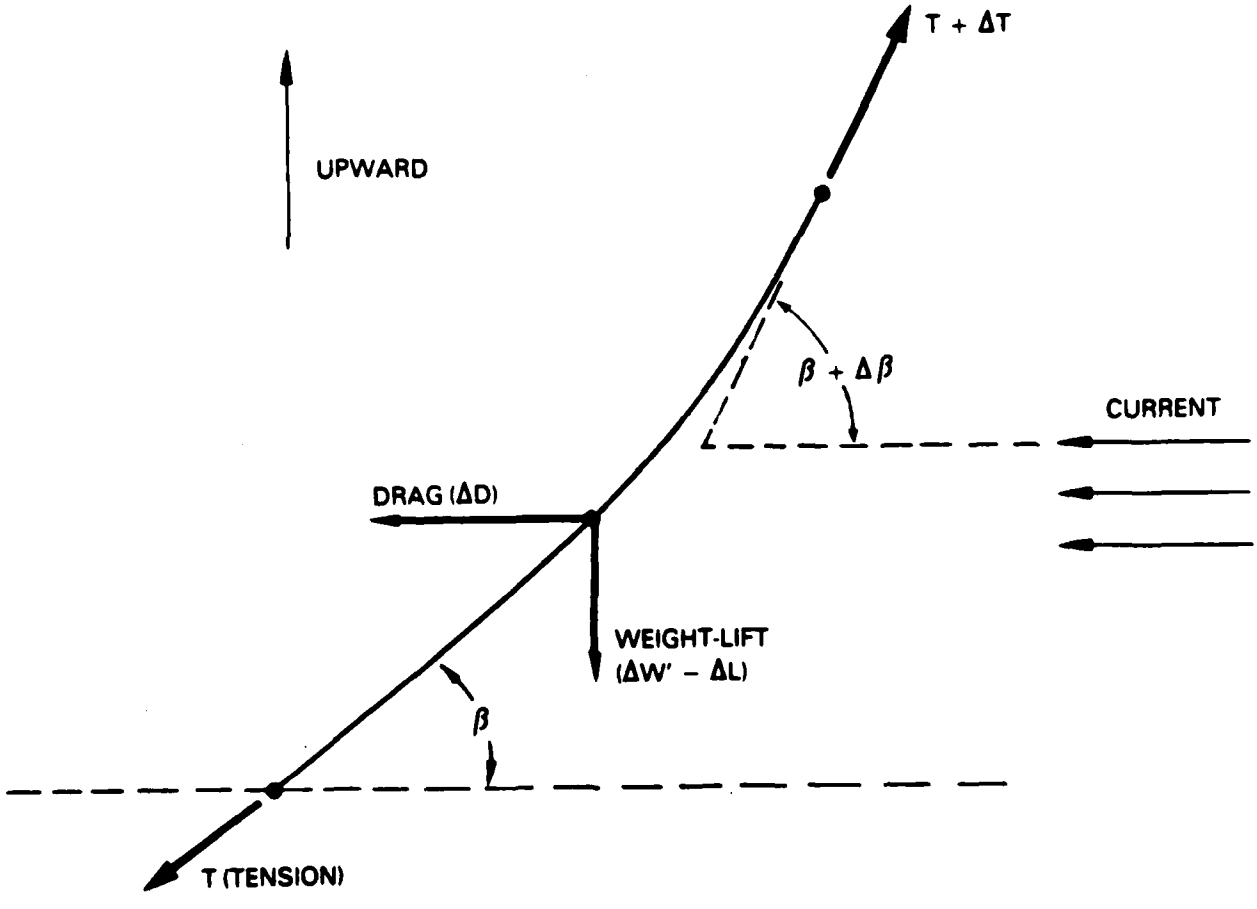

11000-81

Figure A-2. Forces Acting on a Cable Segment in a Flow — $\Delta\beta$ is assumed small over the length of the segment. Magnitudes are for demonstration and are not necessarily drawn to correct scales.

where q is the dynamic pressure (as for the wing), d is the diameter of the cable and $\Delta\ell$ is the length of the cable segment. The drag and lift coefficients, C_D and C_L, are both functions of the cable angle. For bare cable calculations, empirical relations for C_D and C_L were provided by Dr. J. H. Morison (Polar Science Center, University of Washington, Seattle, WA). These are

$$C_D = 0.15 - 0.01697\ \beta + 0.000745\ \beta^2 - 0.000005\ \beta^3 \qquad \text{(A.13)}$$

and

$$C_L = -0.279 + 0.0269\ \beta - 0.000263\ \beta^2, \qquad \text{(A.14)}$$

where β is the cable angle relative to horizontal. For faired cable calculations, the approach of Wingham (1983) was used to determine the effective drag coefficients for the normal and tangential force components.

The bottom-end condition was fixed by specifying both the tension at the platform-end and the angle of the lowermost cable segment relative to horizontal. Next, the program used the solutions for the set of force balance equations to determine the tension and the cable angle that would be necessary at the top-end of the lowermost segment to balance exactly the complement of forces over the segment length. This new tension and angle were then applied as the bottom-end conditions for the next segment above; with the same calculation loop, the new tension and angle at the top of that second segment necessary for a balance of forces were found. The process continued up the cable, producing values for the tension and the cable angle for each successive segment up the cable to the tether point. Horizontal and vertical excursions as a function of distance along the cable were calculated using the respective segment lengths and associated cable angles. Vertical excursions were then used to determine whether or not the particular kite configuration could achieve the sampling goals with the given operating environment.

APPENDIX B

THE FORCE SYSTEM ON THE YO-YO TETHERED PLATFORM

The external forces on the profiler are gravitational forces and contact forces between the platform and the cable and between the platform and the water. The resultant of the former is a weight W acting through the point CM, the center of mass, as shown in Fig. B-1.

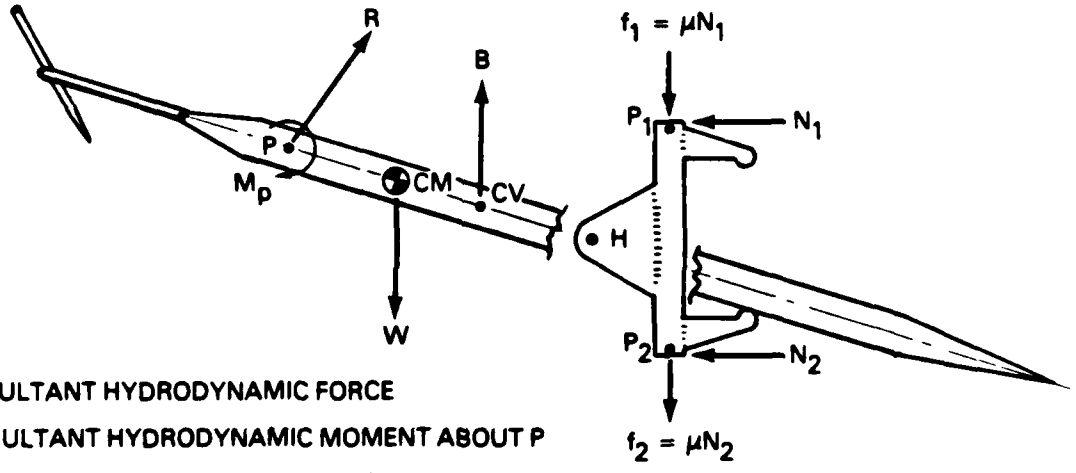

R = RESULTANT HYDRODYNAMIC FORCE

M_p = RESULTANT HYDRODYNAMIC MOMENT ABOUT P

W = RESULTANT GRAVITATIONAL FORCE, THE WEIGHT

B = RESULTANT BUOYANCY FORCE

N_i = CABLE FORCE COMPONENTS NORMAL TO CABLE

f_i = CABLE FORCE COMPONENTS ALONG CABLE

P IS AN ARBITRARY POINT

CM IS THE CENTER OF MASS

CV IS THE CENTER OF VOLUME

P1, P2 ARE CABLE CONTACT POINTS (AT SLIDE BEARINGS)

11000-63

Figure B-1. Forces on the Platform

The contact stresses at the surface interface between the platform and the water are the result of two different mechanisms whose effects are superimposed. The resultant forces due to these stresses are called the buoyancy force and the hydrodynamic force.

For the static case (no motion of the platform through the water), only the buoyancy force occurs. The pressure distribution on the platform results in an upward buoyant force B through the center of volume point CV, as shown in Fig. B-1. This force is the result of the vertical pressure gradient in the water due to gravitation, and has a magnitude equal to the weight of the water displaced, or

$$B = \gamma_w H \tag{B.1}$$

$$H = \text{volume of the platform} \tag{B.2}$$

$$\gamma_w = \text{weight density of the platform} \tag{B.3}$$

When the platform moves through the water, additional surface contact stresses occur. The resultant is called the hydrodynamic force, and it can be represented by a number of equivalent systems of concentrated forces and pitching moment couple systems, as discussed in the following. The stress distribution is equivalent to a resultant hydrodynamic force through a point of action called the center of pressure (a somewhat misleading name since tangential surface stresses have a minor influence on its location), as shown in Fig. B-1. Shifting the force to another point of action requires the addition of a moment couple, as shown in Figs. B-1 and B-2(b). For the latter the point of action is chosen such that the moment does not change with perturbation in angle of attack. This point is called the neutral point. Such a point always exists. In general it moves slightly with angle of attack, but it is usually considered fixed for most analyses. In this case, the neutral point becomes a point about which the pitching moment, M_{NP} is the same at all angles of attack, which accounts for the desirability of using the equivalent system shown in Fig. B-2(b).

Although the location of the neutral point can be considered independent of elevator or wing flap setting with little error, the moment does change with such setting. Because of symmetry, the pitching moment about any point on the platform centerline (which includes the neutral point) vanishes at zero

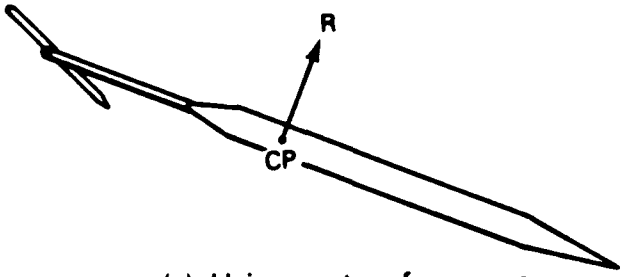

(a) Using center of pressure

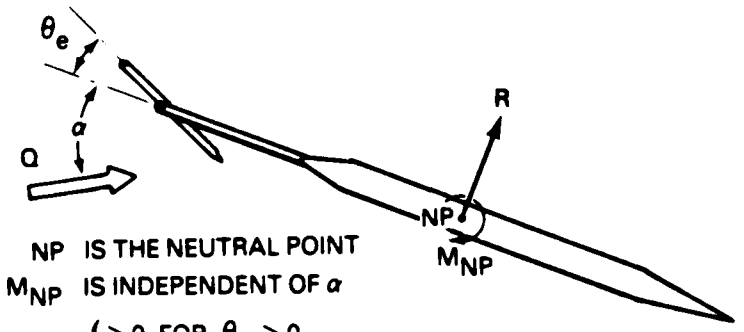

NP IS THE NEUTRAL POINT

M_{NP} IS INDEPENDENT OF α

$$M_{NP} \begin{cases} > 0 \text{ FOR } \theta_e > 0 \\ = 0 \text{ FOR } \theta_e = 0 \\ < 0 \text{ FOR } \theta_e < 0 \end{cases}$$

(b) Using neutral point

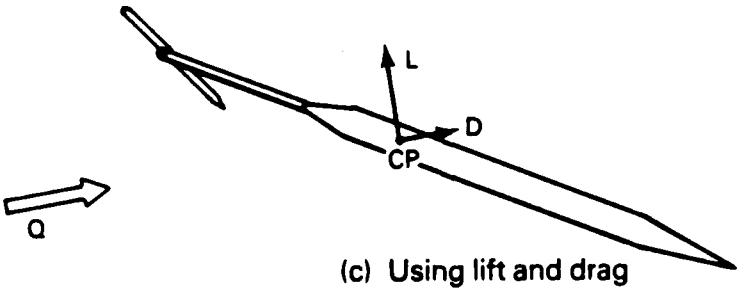

(c) Using lift and drag

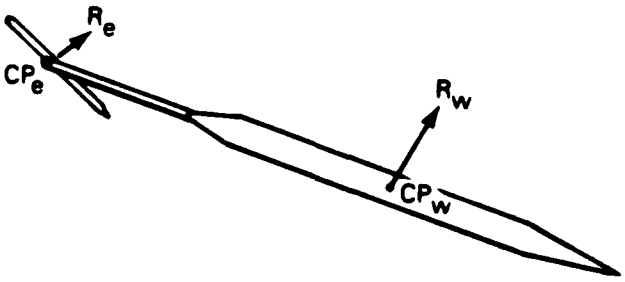

(d) Using center of pressure of each lifting surface

11000-78

Figure B-2. Equivalent Representations of the Hydrodynamic Force

angle of attack and control deflection. Therefore, as illustrated in Fig. B-2(b), for zero control deflection M_{NP} is zero. Similar arguments show that control deflection which provides nose-up moment for the angle of attack for which the resultant force is along the centerline (the zero lift condition) gives positive M_{NP} and vice versa [as indicated in Fig. B-2(b)].

The hydrodynamic force vector is typically specified by orthogonal components. The standard procedure is to use the lift and the drag where the latter is in opposition to the motion of the platform through the water (i.e., along the direction of the current relative to the platform), as shown in Fig. B-2(c).

Finally, another convenient equivalent hydrodynamic force system results from considering the wing and the control surface (canard or tail) separately, as illustrated in Fig. B-2(d). Use of the center of pressure for each lifting element is appropriate, since those points can be assumed to be fixed with little error when symmetric lifting surfaces are utilized. These centers of pressure are designated CP_w and CP_e for the wing and elevator respectively.

The discussion on the external forces operating on the platform is completed by considering the contact forces from the cable which occur at two slip bearings. These contact forces have normal and tangential components, designated N_i and f_i respectively (see Fig. B-1), with the latter opposing motion or impending motion according to

$$|f| \begin{cases} = \mu_d |N| & \text{for motion} \\ < m_s |N| & \text{for impending motion} \end{cases} \tag{B.4}$$

where

$$\mu_d = \text{coefficient of dynamic friction} \tag{B.5}$$

$$\mu_s = \text{coefficient of static friction} \tag{B.6}$$

For pending motion the friction force takes on whatever value is required for equilibrium but cannot exceed the limiting value indicated by Equation (B.1). Fig. B-1 shows the direction of f_i for upward motion either real or impending.

The assembly through which the cable slides is hinged to the platform at point H (see Figs. B-1 and B-3). Note that the hinge point is not necessarily along the cable. If the slider is not included as part of the platform,

contact forces at the stop and at the hinge replace f and N, as shown in Fig. B-3(b). This system is equivalent to that shown in Fig. B-3(c) where the line of action of F_s is shifted to point H and a compensation pitching moment couple, M_s, is added. By considering the slider as a free body of negligible mass and therefore having a negligible inertial force, it can be shown that for the system shown in Fig. B-3(c) the horizontal and vertical contact forces at point H are

$$f = f_1 + f_2 \tag{B.7}$$

$$N = N_1 + N_2 \tag{B.8}$$

The moment M_s is zero when the platform is off of the stop. When the platform is on the stop, the stop force F_s is a constraint force and takes on whatever value is needed for M_s to zero the net moment about the platform center of mass. Also, at all times, the constraint force N takes on whatever value is needed to zero the net horizontal force on the platform.

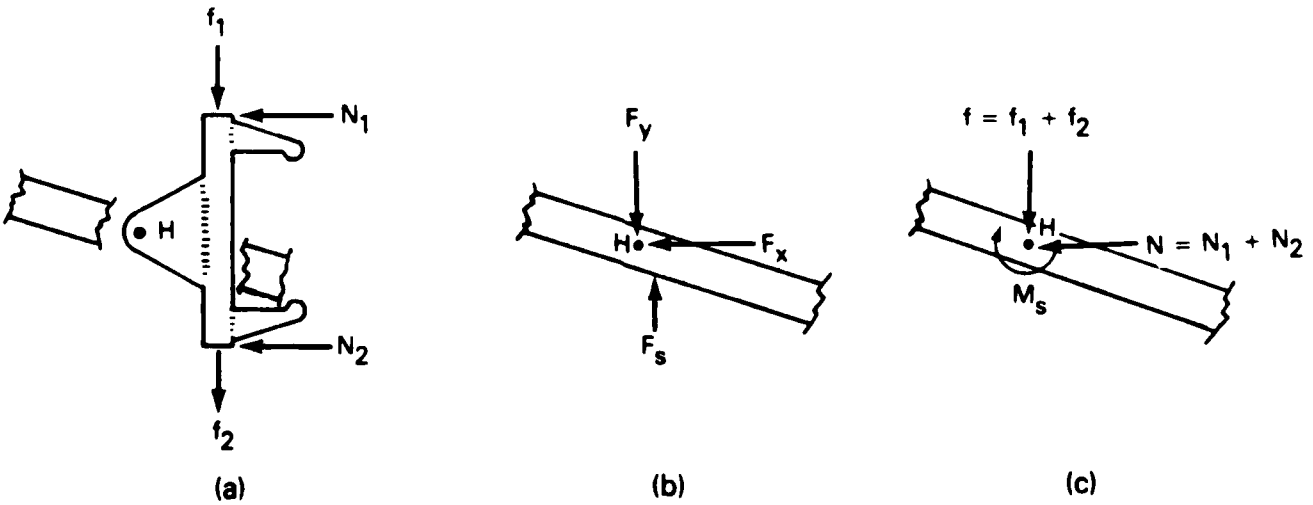

Figure B-3. Equivalent Treatments for the Influence of the Cable Slider

APPENDIX C

THE FLOW TOW TANK FACILITY

Flow Research Company (FLOW) has constructed a modern towing tank system for hydrodynamics and aerodynamics research. The tank is 18.3 meters long, 1.2 meters wide, and 0.91 meter high. It has several special features, including:

(1) Glass side walls and bottom to permit visualization from all directions.

(2) A smooth oil-lubricated carriage (the carriage noise level = 0.1% of the towing speed) to permit accurate velocity control at speeds up to 2.5 m/s.

(3) The tank may be filled with either fresh water or salt water of varying salinity to simulate a variety of atmospheric and oceanographic conditions.

(4) A model can be towed at uniform velocity or in a controlled, cyclic acceleration/deceleration mode.

Experimental investigations with this towing tank system have been published in the open literature and in a series of Flow Research reports and notes.

Experiments are routinely conducted in this tank using probe sensors and flow visualization techniques. At FLOW, we have developed several excellent flow visualization techniques. Conventional dye methods are used routinely to gain qualitative understanding of flow phenomena. Optical methods, such as the shadowgraph technique, are used in a fluid whose density or index of refraction is perturbed by the flow motion. Several novel dye visualization techniques have been developed at FLOW, including the dye-layer technique.

Oscilloscopes - FLOW has several oscilloscopes for studying the characteristics of electrical signals. Among these are a Nicolet Model 4094 digital oscilloscope (manufactured by Nicolet Instrument Corporation, Madison, Wisconsin) and three other Tektronics oscilloscopes.

Digitizer-Microcomputer System - The laboratory is equipped with an ADAC LSI.II minicomputer system for on-line data acquisition and control, and a backup NOVA-800 minicomputer with a 32K core and a number of peripherals. A set of computer programs is available for statistical and spectral analyses of the data.

Data digitization and storage of flow visualization results is accomplished by using a Talos Series 600 digitizing tablet in conjunction with an Apple II Plus Microcomputer. The x and y coordinates of the digitizing pen on the activiated tablet are transmitted serially to the Apple and stored on a floppy disk. Format of data on the Apple random access file consists of a position available for data point indexing in addition to the paired data points on 403 available sectors. The computer has 48K of RAM available for some data analysis programs, which utilize the BASIC language. For the more involved calculations, data can be transferred to the PRIME mainframe computer. Features of the Talos system include the ability to change scale, translate and rotate axes, and enter any ASCII character in addition to the data point coordinates. The latter is a distinct advantage for the indexing of data points on the file. The translucent tablet allows rear projection of a movie frame or 35 mm slide so that data may be directly digitized.

Probe Sensors - Cross-film probes [Thermos-Systems, Inc., (TSI) 1248Y-NACL] connected to 20-channel TSI anemometers (Model 1053B) are available to measure velocity components in a wake. At a speed of 40 cm/s, the frequency response of the probes in water is estimated to be better than 800 Hz, according to the specifications (available from TSI catalog). For measurement of the ambient stratification, a single-electrode conductivity probe, together with a conductivity gauge manufactured by Flow Research Company (Model 1010), may be used. Both sensors have been used for investigating turbulence in stratified flows.

Optical Equipment - FLOW has a collection of available optical equipment and instruments. Included are two 5-W argon-ion lasers, one 5-mW He-Ne laser and accessories for use with LV measurements, flow visualization and developmental work. FLOW also has a large optical table equipped with a set of optical elements including lenses, prisms, beam splitters, colluminators, expanders, mounts, stages and holders.

4591R

END

DTIC

7-86